

Distributed Economic Dispatch for Microgrids Tracking Ramp Power Commands

Hao Tu, *Member, IEEE*, Yuhua Du, *Member, IEEE*, Hui Yu, *Member, IEEE*, Shweta Meena, Xiaonan Lu, *Member, IEEE*, and Srdjan Lukic, *Senior Member, IEEE*

Abstract—When in grid-connected mode of operation, distributed generators (DGs) within the microgrid (MG) can coordinate to act as a single entity to provide services to the bulk grid. The DGs can coordinate their power production to minimize the total operating cost, which is known as the distributed economic dispatch. Various methods have been proposed to solve the MG economic dispatch problem (EDP) in a distributed fashion, under the assumption that DGs’ power output, in aggregate, follows a constant or slowly varying power command. However, when the MG is providing frequency regulation service, or the internal load is highly dynamic, the MG EDP becomes dynamic, and the state-of-the-art distributed approaches cannot guarantee optimality. In this paper, we propose a distributed economic dispatch algorithm for MGs providing frequency regulation service, as an example of a dispatch profile with ramp commands. A consensus protocol guaranteeing zero steady-state error for ramp inputs is integrated into the EDP to find the optimal solution in a distributed way. With the proposed algorithm, the MG is able to tightly follow a time-varying regulation signal while maintaining an optimal economic dispatch for all the DGs within. We validate the proposed method using regulation signals from PJM and demonstrate the algorithm on a hardware-in-the-loop testbed.

Index Terms—Consensus algorithm, distributed control, economic dispatch, microgrid, ramp input, regulation service.

I. INTRODUCTION

MICROGRIDS (MGs) can effectively integrate and manage the ever-increasing number of distributed generators (DGs) in the distribution system. A MG is defined as “a group of interconnected loads and DGs within clearly defined electrical boundaries that acts as a single controllable entity with respect to the grid” [1]. This definition highlights the two key properties of a MG: (1) to the grid, the MG is a single controllable entity and (2) inside the MG, multiple loads and sources interact with each other to achieve stable and economic operation in a self-organized way.

Microgrids can be controlled to provide various services to the grid, including reactive power support, load following, reserve service, frequency regulation service, etc. [2]–[4] by controlling the power exchange at the point of interconnection (POI). Frequency regulation service is one such ancillary service that helps the utility balance the generation and load in real-time and, thus, regulate the grid frequency. The participating resources adjust their output or consumption in response to a signal, referred to as the “regulation signal”, offsetting the power flow at the POI in accordance to the regulation signal in real-time.

This paper is based upon work supported by the United States Army Corps of Engineers under Contract No. W912HQ20C0040. Any opinions, findings and conclusions or recommendations expressed in this paper are those of the author(s) and do not necessarily reflect the views of the United States Army Corps of Engineers.

While providing services to the grid as a single entity, MGs should economically dispatch all the DGs within. The economic dispatch problem (EDP) has a long history in power system applications with centralized control [5]. When the number of DGs in the MG is small, the well-established centralized EDP solutions provide a simple and yet effective way to optimally dispatch the available MG DG resources. However, the centralized control paradigm is challenged by the large-scale integration of DGs. First, the centralized control presents a communication bottleneck in the system, where all information needs to flow to and from a single node. Second, solving the EDP in one central controller makes the MG vulnerable to single point of failure. Third, centralized control algorithms cannot form ad-hoc groups to reflect system reconfiguration or DGs joining or leaving the MG due to, for example, a DG intermittent failure (so-called “plug and play” concept). Distributed control presents a potential solution to manage the future MGs with a large number of DGs [6]–[8]. Under the distributed control framework, each DG only needs to communicate with its neighbors, and can form dynamic networks to adapt to system reconfiguration or communication bottlenecks. Despite its advantages, there has been a limited adoption of distributed MG controllers in the state-of-the-art implementations. This is mostly a reflection of the relatively simple structures for MGs in operation today. Further, many MG designs are built around a single large-capacity device such as a large battery energy storage system (BESS), a design that lends itself to control implementation centralized around that device. In addition, distributed control requires peer-to-peer communication between the DGs, and there is limited adoption of such communication protocols in the power system domain at this time.

Many distributed control algorithms have been proposed for various MG applications, including economic dispatch. In [9], the EDP for a hybrid AC/DC microgrid is formulated and a distributed solution based on the subgradient method is proposed. In [10], a distributed control method based on consensus algorithm is proposed, where all the nodes reach the same optimal incremental cost, with a leader node receiving information about the total load. Another consensus-based EDP solution is proposed in [11] for DC MGs; the proposed algorithm uses the difference between the current reference and measurement in the droop-controlled converters to estimate the MG total load locally, thus eliminating the leader node. A similar method for AC MGs [12] calculates the difference between the active power reference and measurement to estimate the total load. Considering the fact that generation/load imbalance is equivalent to frequency deviation in an islanded microgrid, [13] and [14] use frequency deviation

as input to the incremental cost consensus algorithm. The method eliminates the generation/load imbalance, and thus the frequency deviation in an islanded MG, while reaching optimal incremental cost. Since frequency can be measured locally, the methods in [13] and [14] do not require any load measurement. To avoid instability due to small frequency differences measured by each DER, the algorithm is disabled when the system frequency is close to the rated value [14]. The work in [15] modifies the consensus protocol by adding a new consensus variable. The load information is stored in the initial condition of the new variable. This consensus protocol is called “surplus consensus” in [16] and it can be further improved with random gains to preserve the individual node’s privacy [17], [18].

The state-of-the-art distributed EDP solutions [10]–[15], [17] use the dynamic consensus protocol, and assume the dispatch command (which is the sum of all DGs’ power output) for the MG is either constant [15], [17] or varies slowly [10]–[14]. This assumption is necessary to arrive at the optimal incremental cost because the dynamic consensus protocol can only track the average of constant/step inputs and slowly varying inputs with zero steady-state error [19]. Therefore, the sum of all DGs’ power output has to be constant or vary slowly for the dynamic consensus protocol to converge correctly and to arrive at the optimal incremental cost; otherwise it delivers a sub-optimal solution. The work in [20] discusses the EDP when the sum of all DGs’ power output follows a time-varying load profile and concludes that load mismatch can be eliminated if the rate of change of the system load is lower than the exponential convergence rate of the controller; however, the optimality of the EDP solution cannot be guaranteed.

The limitation of distributed methods originates from the underlying consensus protocols, and, depending on the consensus protocol used, different limitations are present when dealing with time-varying inputs. Dynamic consensus proposed in [19] tracks the average value of inputs if the inputs have at most one pole at the origin, which includes constant/step inputs. For inputs with more than one pole at the origin (e.g., ramp inputs) dynamic consensus has a steady-state error whose value depends on the communication topology. Additionally, dynamic consensus requires the initial values of the consensus variables to equal to that of the inputs. In [21]–[23], robust consensus is proposed, which guarantees convergence to the average from arbitrary initial conditions using an integrator. The authors further present the general form of robust consensus in [24]. By increasing the number of integrators, one form of robust consensus can track ramp inputs with zero steady-state error [24]. However, it requires three integrators, resulting in undesired dynamics and complicated design procedure. Also, in robust consensus, inputs are only enforced on part of the internal states. This creates a low pass filter effect that slows down the tracking speed. Finite time consensus [25] [26] is able to track the average of any time-varying signals with bounded derivatives with zero steady-state error. The major disadvantage of finite time consensus is its convergence speed and chattering phenomenon.

This paper presents a distributed economic dispatch method for MGs tracking ramp power commands. Regulation service

is selected as an example due to its dynamic dispatch profile, which includes ramp regions, requiring continuous adjustment of the power flow at the POI of the MG. The proposed method effectively follows ramp dynamics seen in the frequency regulation service signal. Similar dynamics can be observed in MGs with significant PV generation [27]; aggregated load behavior may also exhibit ramp power demand [28]. The main contribution of the paper is threefold:

- Inspired by internal model principle, we propose a consensus protocol that tracks the average of inputs having two or less poles at the origin including ramp inputs with zero steady-state error. Mathematical proof demonstrates its stability and zero steady-state error with ramp inputs.
- By applying the proposed consensus protocol to the MG EDP, we present a distributed control algorithm that achieves optimal economic dispatch while the MG is providing regulation service. With the proposed algorithm, two goals are achieved simultaneously: 1) the power flow at the MG POI follows the regulation signal tightly to provide satisfactory regulation service; 2) the incremental costs for all DGs reach the optimal value for most regions of the regulation signal, which cannot be achieved by the state-of-the-art distributed approaches based on dynamic consensus. Further, we provide an equivalent model and control gain design procedure for the proposed algorithm.
- The proposed algorithm is implemented on hardware controllers with practical communication networks. Its performance is evaluated against the PJM regulation service profile. With the proposed algorithm, a performance score of 0.9488 is achieved, which satisfies PJM’s requirement for a score of 0.75 or better. We further compare it with the state-of-the-art distributed control algorithm based on dynamic consensus to demonstrate its advantages.

The rest of this paper is organized as follows. In Section II, we formulate the EDP for MGs providing regulation service. Section III presents the proposed consensus protocol and its detailed analysis. In Section IV, we present a distributed EDP solution for MGs providing regulation service by applying the proposed protocol. Section V validates the performance of the proposed method by hardware-in-the-loop (HIL) simulation. Section VI concludes the paper.

II. PROBLEM STATEMENT

A. Regulation Service

Regulation service requires the resources to tightly track the regulation signal. Taking the regulation market hold by PJM as an example [29], two types of regulation signals exist:

- 1) Regulation D (RegD) is a fast and dynamic signal that demands instantaneous response from resources.
- 2) Regulation A (RegA) is a slower signal that aims at stabilizing larger and longer fluctuations at system level.

Fig. 1 shows the normalized test RegD and RegA signal from PJM. Clearly, RegD has a faster rate of change and is more dynamic than RegA, making it more challenging for a MG to follow. In the rest of the paper, we use RegD as the regulation signal. It can be observed that RegD has many regions that require the resource power to ramp up or ramp

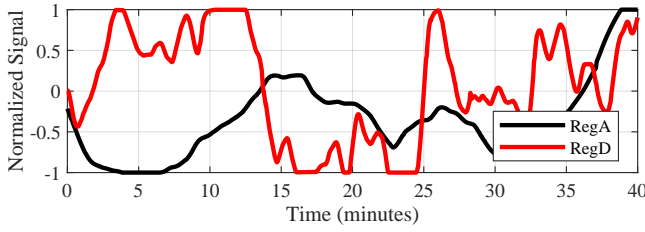


Fig. 1: Test RegA and RegD signal from PJM

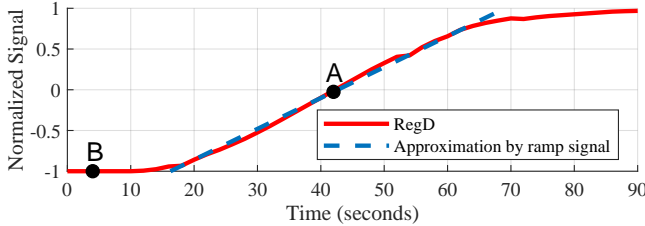


Fig. 2: Fast changing region of RegD around $t = 25$ min and its approximation by a ramp signal

down to support grid frequency regulation, e.g., the regions around $t = 2$ min, $t = 14$ min, $t = 25$ min, $t = 33$ min, etc. Fig. 2 shows RegD around $t = 25$ min where RegD has the largest absolute rate of change. During this region, RegD with a slope of 0.0435 per second at point A can be approximated by a ramp signal, which motivates the development of a consensus protocol that can achieve zero steady-state error for both step/constant inputs (point B) and ramp inputs (point A). It is worth noting that in practice, the RegD signal is received from PJM every 2 seconds. As a result, RegD is a discrete signal with a 2-second time step. In the following we will use a continuous ramp signal instead of a discretized ramp signal for analysis purposes. In the experiment results, we will show that the proposed algorithm can achieve satisfactory performance for both continuous and discretized ramp signals.

B. Microgrid EDP While Providing Regulation Service

In this work, the operating cost of a single DG is approximated by a quadratic function of its output power [5], [30]:

$$f_i(P_i) = a_i P_i^2 + b_i P_i + c_i \quad (1)$$

where P_i is the power output of the i th DG; $P_i > 0$ if the DG injects power into the MG and $P_i < 0$ if the DG draws power from the MG. The cost function coefficients a_i , b_i , and c_i are positive. For a fuel-based DG, such as a diesel generator, $P_i > 0$ since it can only output power. Its cost function coefficients can be directly associated with fuel consumption rate and fuel price [5]. For a DG with storage such as a BESS, $P_i > 0$ means the BESS is discharging and providing power to the MG, while $P_i < 0$ means it is being charged and absorbing power from the MG. The cost function of the BESS $f_i(P_i)$ can be negative for $P_i < 0$. The incremental cost of a DG is given by $\lambda_i(P_i) = df_i/dP_i = 2a_i P_i + b_i$. Fig. 3 shows the typical cost functions and incremental cost functions for a fuel-based DG and a BESS. In Fig. 3, $P_{i,min}$ and $P_{i,max}$ are the minimum and maximum power constraints of the i th DG, respectively. More discussion about the cost functions can be found in [31].

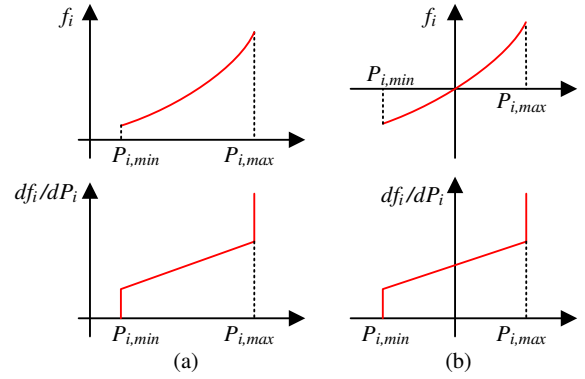


Fig. 3: Cost functions f_i and increment costs df_i/dP_i for (a) a generator and (b) a BESS.

We define the MG net load D as,

$$D = D_L - P_{RES} \quad (2)$$

where D_L is total load in the MG and P_{RES} is the total generation from the non-dispatchable sources such as PV and wind, which operate at their maximum power point. For a MG with N DGs, the EDP when considering regulation service can be formulated as follows:

$$\begin{aligned} & \min_{P_1, \dots, P_N} \sum_i^N f_i(P_i) \\ & \text{subject to } P_1 + \dots + P_N = D - P_{REG} \\ & P_{REG} = B + C_{REG} \text{RegD} \\ & P_{i,min} \leq P_i \leq P_{i,max} \end{aligned} \quad (3)$$

where P_{REG} is the power command calculated from the RegD signal; B is the MG scheduled base load from the grid; C_{REG} is the MG regulation service capacity and RegD is the normalized RegD signal as shown in Fig. 1. The MG imports power from the grid if $P_{REG} > 0$ and exports power if $P_{REG} < 0$. It is assumed that the DGs combined have enough power to satisfy the microgrid load and provide regulation service, i.e.,

$$\sum_i^N P_{i,min} \leq D - P_{REG} \leq \sum_i^N P_{i,max} \quad (4)$$

Otherwise, there exists no solution to problem (3). This assumption also implies that there exists at least one DG that does not reach its power limit.

Problem (3) incorporates the power balance constraints and capacity constraints explicitly and the SoC constraints implicitly (see Remark 1). Other types of constraints, such as ramp rate constraints or line constraints, are not considered for the algorithm proposed in this paper. It remains our future work to develop more general algorithms with various types of constraints.

Remark 1: During operation, an external MG energy management system (EMS) can set the target battery state of charge (SoC) for the BESS [32]. Specifically, the cost function coefficients for the BESS can be generated by a higher-level optimization algorithm running on the EMS [33]. To demonstrate this approach, in this paper, the coefficients a_i , b_i , and c_i for the BESS are functions of the battery SoC. When

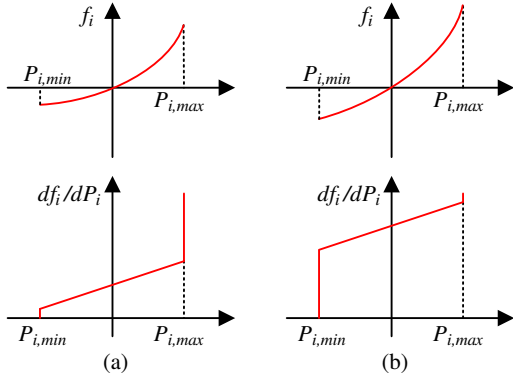


Fig. 4: Cost functions f_i and increment costs df_i/dP_i for a BESS with (a) a high SoC and (b) a low SoC.

the SoC is high, the cost of the BESS is low and thus the BESS tends to discharge. Conversely, when the SoC is low, the cost of the BESS is high and thus the BESS tends to charge. Fig. 4 shows the cost functions and incremental cost functions for a BESS with different SoC levels. At a large time scale, the coefficients are time-varying and properly maintain the SoC around the target. Because the coefficients and the SoC only vary slowly in time, they can be treated as constant at the time scale (i.e., seconds) in which the proposed algorithm operates. In the following, theoretical analysis is conducted with constant coefficients. In the experiment results, we show that the proposed algorithm can achieve satisfactory performance when considering the DG with constant coefficients and the BESS with varying coefficients.

III. CONSENSUS PROTOCOL FOR RAMP INPUTS

In this section, we propose a consensus protocol that tracks the average of ramp inputs with zero steady-state error. In the next section, the proposed protocol is used to develop an distributed EDP algorithm for MGs providing regulation service. The EDP algorithm aims at two goals: 1) controlling the power exchange at the POI of the MG to follow its reference value; 2) distributing the total generation among the DGs so that all the DGs have the same incremental cost, thus satisfying the EDP.

A. Preliminaries on Graph Theory and Dynamic Consensus

Consensus algorithms are widely used for multi-agent systems (MAS) to reach agreement among agents using a sparse communication network. The communication network of a MAS can be modeled by a graph, $G = (V, \mathcal{E}, \mathbf{W})$ where $V = \{v_1, v_2, \dots, v_N\}$ denotes the set of agents; $\mathcal{E} \subseteq V \times V$ denotes the communication links between the agents and \mathbf{W} is the adjacency matrix defined as $w_{ij} = 1$ if and only if the edge $\{v_i, v_j\} \in \mathcal{E}$, otherwise $w_{ij} = 0$. In this work, we assume an undirected graph, i.e. $w_{ij} = w_{ji} = 1$. If there exists a path from any node v_i to any other node v_j in the communication network, the graph is said to be connected.

The Laplacian matrix \mathbf{L} of G is defined as,

$$l_{ij} = \begin{cases} \sum_{k=1, k \neq i}^N w_{ik} & i = j \\ -w_{ij} & i \neq j \end{cases} \quad (5)$$

To track the average of the agents' inputs, dynamic consensus was originally proposed as [19]:

$$\dot{x}_i(t) = -\alpha \sum_{i,j \in \mathcal{E}} w_{ij} [x_i(t) - x_j(t)] + \dot{u}_i(t) \quad (6)$$

where $x_i(t)$ is the agent's observation state; $u_i(t)$ is the local input whose average is of interest; $\alpha > 0$ is a consensus control gain; $u_i(0)$ is the initial value of $u_i(t)$. In [19] Spanos et al. show that as long as the initial condition satisfies $x_i(0) = u_i(0)$, the following statements are true,

- 1) The dynamic consensus algorithm (6) is stable and converge to a steady state;
- 2) Each agent tracks the average of inputs with zero steady-state error for inputs with at most one pole at the origin,

$$\lim_{t \rightarrow \infty} \left(x_i(t) - \frac{1}{N} \sum_{k=1}^N u_k(t) \right) = 0$$

if input $u_k(t)$ is a step or constant signal for any k .

By introducing an intermediate variable $p_i(t) = u_i(t) - x_i(t)$, (6) can be rewritten as,

$$\dot{p}_i(t) = -\alpha \sum_{i,j \in \mathcal{E}} w_{ij} [x_i(t) - x_j(t)] \quad (7)$$

$$x_i(t) = u_i(t) - p_i(t) \quad (8)$$

When implemented in practical controllers, the advantages of using (7) and (8) instead of (6) are: 1) the initial condition can be easily satisfied by setting $p_i(0) = 0$; 2) the need for the derivative of the input $\dot{u}_i(t)$ is eliminated. The second point is important in practical implementation because derivatives are sensitive to noise and may destabilize the controllers.

B. Proposed Consensus Protocol

Although dynamic consensus (6) works well for step signals or constant signals, it has steady-state error for ramp inputs, which has two poles at the origin. If we use (6) to track the RegD signal, the result will be inaccurate during the ramp regions. According to internal model principle, a controller achieves zero steady-state error for an input if it includes the model of that input. For ramp inputs with two poles at the origin, two integrators are necessary. To that end, we propose consensus protocol (9) and (10) to track the average of ramp inputs with zero steady-state error. In the following we drop time argument t for brevity.

$$\dot{x}_i = -\alpha \sum_{i,j \in \mathcal{E}} w_{ij} (x_i - x_j) - \beta \sum_{i,j \in \mathcal{E}} w_{ij} (y_i - y_j) + \dot{u}_i \quad (9)$$

$$\dot{y}_i = -\beta \sum_{i,j \in \mathcal{E}} w_{ij} (y_i - y_j) + \dot{u}_i \quad (10)$$

where x_i and y_i are internal states; α and β are control gains. It is required that the initial condition satisfies $x_i(0) = y_i(0) = u_i(0)$. Compared to (6), protocol (9) and (10) uses two integrators to calculate x_i . According to internal model principle, the proposed consensus protocol can achieve zero steady-state error for inputs having two or less poles at the origin, which include step/constant inputs and ramp inputs.

Above equations can be written in matrix form,

$$\dot{\mathbf{s}} = \mathbf{A}\mathbf{s} + \mathbf{B}\mathbf{u} \quad (11)$$

$$\mathbf{z} = \mathbf{C}\mathbf{s} \quad (12)$$

where $\mathbf{A} = \begin{bmatrix} -\alpha\mathbf{L} & -\beta\mathbf{L} \\ \mathbf{0}_{N \times N} & -\beta\mathbf{L} \end{bmatrix}$, $\mathbf{B} = \begin{bmatrix} \mathbf{I}_N \\ \mathbf{I}_N \end{bmatrix}$, $\mathbf{C} = [\mathbf{I}_N \quad \mathbf{0}_{N \times N}]$, and $\mathbf{s} = [\mathbf{x}^T \quad \mathbf{y}^T]^T$. \mathbf{x} , \mathbf{y} , and \mathbf{u} are the column vectors for x_i , y_i and u_i , respectively. \mathbf{z} is the observation vector. \mathbf{I}_N is the N dimensional identity matrix, and $\mathbf{0}_{N \times N}$ is a $N \times N$ matrix with all zero elements.

To track the average of inputs, the observation vector \mathbf{z} should converge to,

$$\mathbf{z} = \mathbf{z}^* = \frac{1}{N} \mathbf{1}\mathbf{1}^T \mathbf{u} \quad (13)$$

where $\mathbf{1}$ is a N dimensional vector with all elements being 1.

Like in the case of dynamic consensus, it is preferable to define intermediate variables $p_i^x(t) = u_i(t) - x_i(t)$ and $p_i^y(t) = u_i(t) - y_i(t)$ when implementing the proposed protocol in practical controllers. This allows the initial condition to be easily satisfied and eliminates the need to compute the derivative of the input $\dot{u}_i(t)$.

C. Convergence Analysis

In what follows, we first prove the stability of the proposed protocol (11). Then, we show that it achieves zero steady-state error for ramp inputs. Finally, we analyze its convergence speed and discuss its parameter design.

For an undirected and connected graph, \mathbf{L} is a symmetric matrix. It has N eigenvalues with $0 = \psi_1 < \psi_2 \leq \psi_3 \leq \dots \leq \psi_N$. With diagonal matrix $\Psi = \text{diag}(\psi_1, \dots, \psi_N)$ and orthonormal eigenbasis $\mathbf{Q} = [\mathbf{q}_1, \dots, \mathbf{q}_N]$, \mathbf{L} can be written as $\mathbf{L} = \mathbf{Q}\Psi\mathbf{Q}^T$. Also, we have $\mathbf{Q}^{-1} = \mathbf{Q}^T$ because \mathbf{L} is symmetric. It is easy to verify that $\mathbf{q}_1 = \frac{1}{\sqrt{N}}\mathbf{1}$ is the right eigenvector for $\psi_1 = 0$. The eigenvalues of \mathbf{A} can be found by,

$$\begin{aligned} \xi\mathbf{I}_{2N} - \mathbf{A} &= \begin{bmatrix} \xi\mathbf{I}_N + \alpha\mathbf{L} & \beta\mathbf{L} \\ \mathbf{0}_{N \times N} & \xi\mathbf{I}_N + \beta\mathbf{L} \end{bmatrix} \\ &= \mathbf{Q} \begin{bmatrix} \xi\mathbf{I}_N + \alpha\Psi & \beta\Psi \\ \mathbf{0}_{N \times N} & \xi\mathbf{I}_N + \beta\Psi \end{bmatrix} \mathbf{Q}^T = \mathbf{Q}\mathbf{S}\mathbf{Q}^T \end{aligned} \quad (14)$$

We have $\det(\xi\mathbf{I}_{2N} - \mathbf{A}) = \det(\mathbf{S})$ from (14), and because \mathbf{S} is a upper triangular matrix, it is easy to conclude that the eigenvalues of \mathbf{A} are,

$$\xi_{2i-1} = -\alpha\psi_i, \quad \xi_{2i} = -\beta\psi_i \quad (i = 1, 2, 3, \dots, N) \quad (15)$$

Recall for an undirected connected graph, $\psi_1 = 0$ and $\psi_i > 0$ for $i = 2, 3, \dots, N$. Therefore, \mathbf{A} has two zero eigenvalues $\xi_1 = \xi_2 = 0$, and the remaining eigenvalues (ξ_3, \dots, ξ_{2N}) are negative. The system (11) is bounded-input, bounded-output (BIBO) stable.

Next, we will show that (11) tracks the average of ramp inputs with zero steady-state error. To do that, we first take the Laplace transform of (11) and write the output-to-input

transfer function as,

$$\begin{aligned} \mathbf{T}(s) &= \frac{\mathbf{Z}(s)}{\mathbf{U}(s)} = s\mathbf{C}(s\mathbf{I}_{2N} - \mathbf{A})^{-1}\mathbf{B} \\ &= s \begin{bmatrix} \mathbf{I}_N & \mathbf{0}_{N \times N} \\ \mathbf{0}_{N \times N} & s\mathbf{I}_N + \beta\mathbf{L} \end{bmatrix}^{-1} \begin{bmatrix} s\mathbf{I}_N + \alpha\mathbf{L} & \beta\mathbf{L} \\ \mathbf{0}_{N \times N} & s\mathbf{I}_N + \beta\mathbf{L} \end{bmatrix} \begin{bmatrix} \mathbf{I}_N \\ \mathbf{I}_N \end{bmatrix} \\ &= \sum_{i=1}^N \frac{s^2}{(s + \alpha\psi_i)(s + \beta\psi_i)} \mathbf{q}_i \mathbf{q}_i^T \end{aligned} \quad (16)$$

Derivation of (16) is presented in Appendix A. Recall $\psi_1 = 0$ and $\mathbf{q}_1 = \frac{1}{\sqrt{N}}\mathbf{1}$, $\mathbf{T}(s)$ can be written as,

$$\mathbf{T}(s) = \frac{1}{N} \mathbf{1}\mathbf{1}^T + \sum_{i=2}^N \frac{s^2}{(s + \alpha\psi_i)(s + \beta\psi_i)} \mathbf{q}_i \mathbf{q}_i^T \quad (17)$$

We define the error function as

$$\mathbf{e} = \mathbf{z} - \mathbf{z}^* = \mathbf{z} - \frac{1}{N} \mathbf{1}\mathbf{1}^T \mathbf{u} \quad (18)$$

Substituting $\mathbf{Z}(s) = \mathbf{T}(s)\mathbf{U}(s)$ and (17) into (18),

$$\mathbf{E}(s) = \sum_{i=2}^N \frac{s^2}{(s + \alpha\psi_i)(s + \beta\psi_i)} \mathbf{q}_i \mathbf{q}_i^T \mathbf{u} \quad (19)$$

According to *Final Value Theorem*, for any \mathbf{u} having two or less poles at the origin, the steady-state error will be zero. Particularly, for ramp inputs $\mathbf{U}(s) = \mathbf{K}/s^2$ with $\mathbf{K} = [k_1, \dots, k_n]^T$ being a constant vector, we have,

$$\begin{aligned} \lim_{t \rightarrow \infty} \mathbf{e} &= \lim_{s \rightarrow 0} s\mathbf{E}(s) \\ &= \lim_{s \rightarrow 0} \sum_{i=2}^N \frac{s^3}{(s + \alpha\psi_i)(s + \beta\psi_i)} \mathbf{q}_i \mathbf{q}_i^T \frac{\mathbf{K}}{s^2} = \mathbf{0} \end{aligned} \quad (20)$$

This completes the proof that the proposed consensus protocol (11) is stable, and can track the average of ramp inputs with zero steady-state error.

Next, we study the convergence speed of the proposed protocol and provide some design considerations for α and β . To simplify the analysis, we assume the inputs are one of the following signals: 1) step signals; 2) constant signals. For above signals, we have $\dot{u} \approx 0$ and $\frac{1}{N}\mathbf{1}\mathbf{1}^T \mathbf{u}$ is a constant for $t > t_0$. We rewrite the proposed consensus protocol (9) and (10) as

$$\dot{x}_i = -\alpha \sum_{j \in \mathcal{E}} w_{ij} (x_i - x_j) + \dot{y}_i \quad (21)$$

$$\dot{y}_i = -\beta \sum_{j \in \mathcal{E}} w_{ij} (y_i - y_j) + \dot{u}_i \quad (22)$$

Eq. (22) indicates that in terms of tracking the average of input u_i , the equation governing the state y_i is the same as the one for dynamic consensus (6). The equation governing the state x_i represents another dynamic consensus that tracks the average of y_i . The proposed protocol can be seen as the cascade of two dynamic consensus protocols. The convergence speed of x_i tracking the average of u_i is a combined result of 1) the convergence speed of y_i tracking the average of u_i and 2) the convergence speed of x_i tracking the average of y_i .

We define the disagreement vector as,

$$\delta = \begin{bmatrix} \delta_x \\ \delta_y \end{bmatrix} = \begin{bmatrix} \mathbf{x} - \frac{1}{N} \mathbf{1}\mathbf{1}^T \mathbf{u} \\ \mathbf{y} - \frac{1}{N} \mathbf{1}\mathbf{1}^T \mathbf{u} \end{bmatrix} \quad (23)$$

Substituting (23) into (11) to get the disagreement dynamics,

$$\begin{bmatrix} \dot{\delta}_x \\ \dot{\delta}_y \end{bmatrix} = \begin{bmatrix} -\alpha\mathbf{L} & -\beta\mathbf{L} \\ \mathbf{0}_{N \times N} & -\beta\mathbf{L} \end{bmatrix} \begin{bmatrix} \delta_x \\ \delta_y \end{bmatrix} = \mathbf{A} \begin{bmatrix} \delta_x \\ \delta_y \end{bmatrix} \quad (24)$$

Eq. (24) describes the dynamics of the disagreement vector and it can be used to determine the convergence speed of x_i and y_i tracking the average of u_i . The dynamics of δ_y are decoupled from δ_x . In [34], it is shown that the convergence speed of average consensus (thus the convergence speed of δ_y) is governed by the second largest eigenvalue of $-\beta\mathbf{L}$, i.e. $-\beta\psi_2$. Because x_i tracks the average of y_i , x_i cannot reach steady state before y_i does. Therefore, the convergence speed of x_i cannot be faster than that of y_i . In other words, the upper limit of the convergence speed of x_i is set by β . Here we consider that ψ_2 is the property of the communication network and cannot be changed.

From (21), it can be observed that α determines the speed of x_i tracking the average of y_i . On one hand, a small α will reduce the overall convergence speed because x_i can only track the average of y_i slowly even if y_i has reached steady state. On the other hand, if α is large, the speed of x_i tracking the average of y_i will be fast. However, it does not improve the overall convergence speed because it is limited by β . We can get the following conclusion regarding the parameters,

- 1) The convergence speed of y is determined by β and the communication topology. The design of β is a trade-off between the convergence speed and stability margin.
- 2) The convergence speed of x is determined by α , β , and the communication topology. One good practice is $\alpha = \beta$.

Although the convergence speed of the proposed protocol (9) cannot be faster than that of the dynamic consensus (6), the main advantage of the proposed protocol is zero steady-state error for ramp inputs.

Remark 2: The proposed consensus protocol (11) and its analysis above do not assume any specific application. It can be used in any application where tracking the average of ramp inputs is desired. In the context of the MG, different distributed control algorithms can be built based on the proposed consensus protocol (11) to realize different control goals. In the next section, we propose a distributed control algorithm based on (11) for the EDP in MGs which allows for minimizing the operating cost while providing regulation service. The proposed algorithm focuses on the grid-connected operation of the MG when it provides regulation service to the grid. While it is possible to build a distributed control algorithm based on (11) for islanded operation, it is not the focus of this paper and will not be further discussed.

IV. DISTRIBUTED ECONOMIC DISPATCH WHILE PROVIDING REGULATION SERVICE

In this section, we first present the proposed distributed control algorithm. Then, we show that the proposed algorithm is stable when considering the feedback from the physical system. Finally, we provide a design method for the control gains which provides a sufficient condition for system stability when considering delay. With the proposed algorithm, the two goals can be decoupled: the proposed consensus protocol (11)

guarantees the reaching of the same incremental cost, while the POI power tracking performance can be adjusted by the control gain.

A. Proposed Distributed EDP Algorithm

To solve the EDP in a distributed way, we apply the dual decomposition to the original problem, which divides the problem into two levels of optimization. At the lower level, each DG solves the following problem locally,

$$P_i^*(\lambda) = \arg \min_{P_i} (f_i(P_i) - \lambda^* P_i) \quad (25)$$

subject to $P_{i,min} \leq P_i \leq P_{i,max}$

With a quadratic cost function f_i , problem (25) can be solved analytically as,

$$P_i^* = \begin{cases} P_{i,max} & \lambda^* \geq \lambda_{i,max} \\ (\lambda^* - b_i)/2a_i & \lambda_{i,min} < \lambda^* < \lambda_{i,max} \\ P_{i,min} & \lambda^* \leq \lambda_{i,min} \end{cases} \quad (26)$$

where $\lambda_{i,min} = 2a_i P_{i,min} + b_i$, $\lambda_{i,max} = 2a_i P_{i,max} + b_i$, and λ^* is the optimal global incremental cost that has to be solved by the higher second level optimization. Conventionally, the second level optimization requires the information from all DGs, loads, and the regulation signal, thus resulting in a centralized solution. To avoid this, we apply the proposed consensus protocol (11) to estimate the optimal global incremental cost by individual DGs. The proposed algorithm is written as,

$$\dot{x}_i = -\alpha \sum_{i,j \in \mathcal{E}} w_{ij} (x_i - x_j) - \beta \sum_{i,j \in \mathcal{E}} w_{ij} (y_i - y_j) - \epsilon_i (P_{REG} - P_{POI}) \quad (27)$$

$$\dot{y}_i = -\beta \sum_{i,j \in \mathcal{E}} w_{ij} (y_i - y_j) - \epsilon_i (P_{REG} - P_{POI}) \quad (28)$$

$$\lambda_i^* = x_i \quad (29)$$

where P_{POI} is the power exchanged at the POI and it can be monitored by the POI relay. The MG imports power if $P_{POI} > 0$, and the MG exports power if $P_{POI} < 0$. ϵ_i is the designed regulation service gain, $\epsilon_i > 0$ if the DG is the regulation service DG, otherwise $\epsilon_i = 0$. To have a meaningful input, we require $\epsilon_i > 0$ for at least one DG. λ_i^* is the agent's local estimation of the optimal global incremental cost. The block diagram of the proposed distributed control algorithm is shown in Fig. 5.

Referring to (9), the consensus tracks the average of input $u_i = \epsilon_i \int (P_{POI} - P_{REG})$. When P_{REG} is calculated from the RegD signal, input u_i will be close to a ramp signal at the fast changing region of RegD, and conventional distributed algorithm based on dynamic consensus (6) will not converge correctly. The proposed EDP algorithm (26)-(29) presents two requirements for the communication network. First, the communication graph among DGs should be connected since it uses the proposed consensus protocol to reach agreement on the incremental cost. Second, at least one of the DGs should be able to receive the RegD signal and POI power measurement. Derivatives are avoided in the proposed algorithm since P_{REG} is received from the communication link and P_{POI} is measured at the POI.

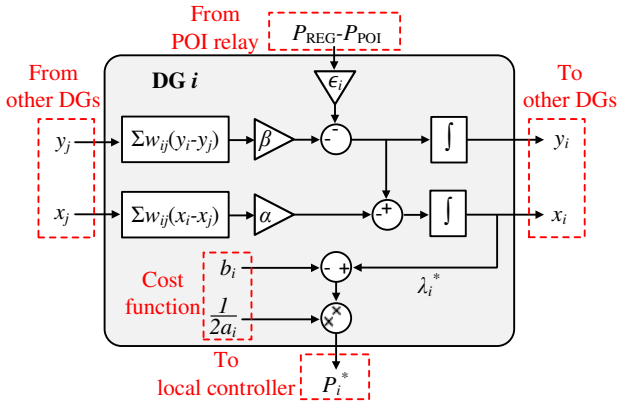


Fig. 5: Block diagram of the proposed distributed control algorithm

B. Stability Analysis

To perform the stability analysis for system (26)-(29), we make the following assumptions.

- 1) The system voltage is well regulated within the tolerance band by the grid and transformers. This assumption is valid because the MG is always connected to grid when providing ancillary service.
- 2) The DGs' lower level dynamics such as voltage and current loop are ignored. This is justified since the proposed control algorithm operates at a much larger time scale and its dynamics are clearly decoupled from the faster dynamics of DGs.
- 3) We also assume that the DG's output can follow their power reference accurately, i.e. $P_i = P_i^*$. At the end of this subsection, we show that the system is stable under a constant offset between the power reference and actual output, i.e., $P_i = P_i^* + \Delta P_i$.

With above assumptions, we can write the power balance equation for the MG,

$$P_{\text{POI}} + \sum_{i=1}^N P_i = D \quad (30)$$

Next, we will discuss the stability for unconstrained case first, i.e., none of the DGs reaches its minimum or maximum power output. Then, we will extend the analysis to the general constrained case.

1) *Unconstrained case*: when none of the DGs reaches its limit, by substituting (26) and (29) into (30) we can write the POI power as,

$$P_{\text{POI}} = D - \sum_{i=1}^N \frac{x_i - b_i}{2a_i} = - \sum_{i=1}^N \frac{x_i}{2a_i} + D' \quad (31)$$

where $D' = D + \sum_{i=1}^N \frac{b_i}{2a_i}$. Substitute (31) into (27) and (28) and write it in matrix form,

$$\begin{bmatrix} \dot{\mathbf{x}} \\ \dot{\mathbf{y}} \end{bmatrix} = \left(\begin{bmatrix} -\alpha \mathbf{L} & -\beta \mathbf{L} \\ \mathbf{0}_{N \times N} & -\beta \mathbf{L} \end{bmatrix} + \begin{bmatrix} -\varepsilon \sigma / 2 & \mathbf{0}_{N \times N} \\ -\varepsilon \sigma / 2 & \mathbf{0}_{N \times N} \end{bmatrix} \right) \begin{bmatrix} \mathbf{x} \\ \mathbf{y} \end{bmatrix} + \begin{bmatrix} \varepsilon \\ \varepsilon \end{bmatrix} (D' - P_{\text{REG}}) \quad (32)$$

where $\varepsilon = [\varepsilon_1 \ \varepsilon_2 \ \dots \ \varepsilon_N]^T$, $\sigma = [\frac{1}{a_1} \ \frac{1}{a_2} \ \dots \ \frac{1}{a_N}]$. The new system matrix (which is the matrix sum in the bracket)

can be viewed as matrix \mathbf{A} being perturbed by another matrix $\mathbf{P} = \begin{bmatrix} -\varepsilon \sigma / 2 & \mathbf{0}_{N \times N} \\ -\varepsilon \sigma / 2 & \mathbf{0}_{N \times N} \end{bmatrix}$. When the control gains ε_i are small and positive, we can analyze the new system matrix by eigenvalue perturbation approach.

As shown in Section III, \mathbf{A} has two zero eigenvalues $\xi_1 = \xi_2 = 0$, and the remaining eigenvalues (ξ_3, \dots, ξ_{2N}) are negative. We construct vector \mathbf{v}_1^T , \mathbf{v}_2^T and \mathbf{w}_1 , \mathbf{w}_2 as,

$$\mathbf{V}^T = \begin{bmatrix} \mathbf{v}_1^T \\ \mathbf{v}_2^T \end{bmatrix} = \begin{bmatrix} \mathbf{1}_{1 \times N} & \mathbf{0}_{1 \times N} \\ \mathbf{0}_{1 \times N} & \mathbf{1}_{1 \times N} \end{bmatrix} / \sqrt{N} \quad (33)$$

$$\mathbf{W} = [\mathbf{w}_1 \ \mathbf{w}_2] = \begin{bmatrix} \mathbf{1}_{N \times 1} & \mathbf{0}_{N \times 1} \\ \mathbf{0}_{N \times 1} & \mathbf{1}_{N \times 1} \end{bmatrix} / \sqrt{N} \quad (34)$$

It can be easily verified that \mathbf{v}_1^T and \mathbf{v}_2^T (\mathbf{w}_1 and \mathbf{w}_2) are two linearly independent left (right) eigenvectors of \mathbf{A} corresponding to the two zero eigenvalues and they satisfy $\mathbf{V}^T \mathbf{W} = \mathbf{I}_N$. If the control gains ε_i are small, the movement of eigenvalues ξ_1 and ξ_2 when \mathbf{A} is perturbed by \mathbf{P} can be quantified by the eigenvalues of $\mathbf{V}^T \mathbf{P} \mathbf{W}$ [35], [36], and we have,

$$\mathbf{V}^T \mathbf{P} \mathbf{W} = \frac{1}{N} \begin{bmatrix} -\mathbf{1}_{1 \times N} \frac{\varepsilon \sigma}{2} \mathbf{1}_{N \times 1} & \mathbf{0} \\ -\mathbf{1}_{1 \times N} \frac{\varepsilon \sigma}{2} \mathbf{1}_{N \times 1} & \mathbf{0} \end{bmatrix} = \begin{bmatrix} p & 0 \\ p & 0 \end{bmatrix} \quad (35)$$

where,

$$p = -\frac{1}{2N} (\varepsilon_1 + \dots + \varepsilon_N) \left(\frac{1}{a_1} + \dots + \frac{1}{a_N} \right) \quad (36)$$

It can be observed from (35) that the eigenvalues of the 2×2 matrix $\mathbf{V}^T \mathbf{P} \mathbf{W}$ are 0 and p . The eigenvalues ξ_1 and ξ_2 after the perturbation moves to ξ_1 and $\xi_2 + p$, respectively. With all $\varepsilon_i \geq 0$ and at least one $\varepsilon_i > 0$, we have $p < 0$ and therefore $\xi_2 + p < 0$. We can find a positive upper bound θ_1 such that $\xi_1 = 0$ and $\xi_2 + p < 0$ for $\varepsilon_i < \theta_1$. Therefore, when ε_i is small, the movement of ξ_1 and ξ_2 will not lead to instability. Next, we consider the movement of all the other negative eigenvalues (ξ_3, \dots, ξ_{2N}) under the perturbation. Because eigenvalues are continuous functions of matrix entries, the eigenvalues continuously depends on control gains ε_i . We can find a positive upper bound θ_2 such that $\text{Re}(\xi_i) < 0$ ($i = 3, 4, \dots, 2N$) for $\varepsilon_i < \theta_2$. As a result, if we select the control gains to satisfy $\varepsilon_i < \text{MIN}(\theta_1, \theta_2)$, the new system matrix will have a simple eigenvalue at zero and all the other eigenvalues are in the open left half-plane. The system is stable.

2) *Constrained case*: if some DGs have reached their minimum or maximum output, their power output becomes constant and will not change with the incremental cost anymore. Thus, the POI power (31) for constrained case becomes,

$$P_{\text{POI}} = D - \sum_{i \in \mathcal{NS}} \frac{x_i - b_i}{2a_i} - \sum_{i \in \mathcal{S}} P_i = - \sum_{i \in \mathcal{NS}} \frac{x_i}{2a_i} + D'' \quad (37)$$

where \mathcal{S} is the index set for saturated DGs that have reached their minimum or maximum output, \mathcal{NS} is the index set for non-saturated DGs, and $D'' = D + \sum_{i \in \mathcal{NS}} \frac{b_i}{2a_i} - \sum_{i \in \mathcal{S}} P_i$. Following the same process as the unconstrained case, we can

get p for constrained case as,

$$p = -\frac{1}{2N}(\epsilon_1 + \dots + \epsilon_N) \sum_{i \in \mathcal{NS}} \frac{1}{a_i} \quad (38)$$

Based on (4), which states that that combined DGs power output exceeds the MG load and regulation command, there is at least one element in \mathcal{NS} . Thus, $p < 0$ is valid for constrained case. By the same argument for unconstrained case, we can conclude that the system is stable when considering the DGs' capacity constraints.

Above proof for both unconstrained and constrained cases does not depend on the voltage, meaning the proposed EDP algorithm is robust against system voltage variations. However, assumption 1) is necessary to avoid trip of and damage to DGs and loads. Further, if there exists a constant offset ΔP_i between the DG's the power reference P_i^* and its actual power output P_i , the proposed control is still stable. This can be shown by writing

$$P_{\text{POI}} + \sum_{i=1}^N P_i = P_{\text{POI}} + \sum_{i=1}^N (P_i^* + \Delta P_i) = D \quad (39)$$

Because ΔP_i is constant, it can be moved to the right side of the equation and combined with the system net load D . Then, all the proof remains the same.

C. Controller Gain Design

In the previous subsection, we showed that the algorithm (26)-(29) is stable for small $\epsilon_i > 0$. In this subsection, we will discuss the design procedure for controller gains ϵ_i when considering practical communication delay.

First, we sum up equation (27) for all DGs,

$$\sum_{i=1}^N \dot{x}_i = -\epsilon_{\text{SUM}}(P_{\text{REG}} - P_{\text{POI}}) \quad (40)$$

where $\epsilon_{\text{SUM}} = \sum_{i=1}^N \epsilon_i$. Note this step uses the conservation property of Laplacian matrix and it is valid no matter whether the consensus has converged or not. Substitute P_{POI} with (31) into (40),

$$\begin{aligned} \sum_{i=1}^N \dot{x}_i &= -\epsilon_{\text{SUM}} \sum_{i=1}^N \frac{x_i(s)}{2a_i} + \epsilon_{\text{SUM}}(D' - P_{\text{REG}}) \\ &= -\epsilon_{\text{SUM}} \frac{\sum_{i=1}^N x_i}{2a_{\text{AVE}}} + \epsilon_{\text{SUM}}(D' - P_{\text{REG}}) \end{aligned} \quad (41)$$

where $a_{\text{AVE}} = \sum_{i=1}^N x_i / \sum_{i=1}^N \frac{x_i(s)}{a_i}$. It is easy to see $a_{\text{MIN}} \leq a_{\text{AVE}} \leq a_{\text{MAX}}$ with $a_{\text{MIN}} = \text{MIN}(a_1, a_2, \dots, a_N)$ and $a_{\text{MAX}} = \text{MAX}(a_1, a_2, \dots, a_N)$. By defining $\chi = \sum_{i=1}^N x_i$, equation (41) becomes,

$$\dot{\chi} = -\epsilon_{\text{SUM}} \frac{\chi}{2a_{\text{AVE}}} + \epsilon_{\text{SUM}}(D' - P_{\text{REG}}) \quad (42)$$

Equation (42) suggests the system dynamics can be modeled by the block diagram shown in Fig. 6 when the dynamics of individual DG are sufficiently fast compared to the ones of ancillary service. The loop gain of Fig. 6 is,

$$T_{\chi}(s) = \frac{\epsilon_{\text{SUM}}}{2a_{\text{AVE}}s} \quad (43)$$

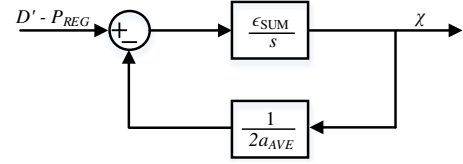


Fig. 6: Equivalent model for designing gain ϵ_i

When (26)-(29) are implemented in DGs, there is inevitably a delay between calculating $(x_i, y_i, \lambda_i^*, P_i^*)$ and monitoring changes in P_{POI} . This delay includes the communication delay, DG control delay, POI relay measurement delay, etc. We lump all the delays into a single one and model it as $T_{\tau}(s) = e^{-s\tau_{\text{MAX}}}$ and τ_{MAX} is the worst case delay in the system. When considering delays, equation (43) becomes

$$T_{\chi}(s) = \frac{\epsilon_{\text{SUM}}}{2a_{\text{AVE}}s} e^{-s\tau_{\text{MAX}}} \quad (44)$$

Note,

$$|T_{\chi}(s)| \leq \left| \frac{\epsilon_{\text{SUM}}}{2a_{\text{MIN}}s} \right| \quad \angle T_{\chi}(s) = -\pi/2 - s\tau_{\text{MAX}} \quad (45)$$

Equation (44) and (45) suggest that the sum of controller gains ϵ_{SUM} determines the system's tracking performance and stability with delay while the value of individual gain ϵ_i is not important in this respect. To derive (42) and the equivalent model in Fig. 6, it is not necessary that the consensus protocol has converged, i.e., $x_1 = x_2 = \dots = x_i$. This means that the performance of P_{POI} tracking P_{REG} is decoupled from the performance of all agents reaching the same optimal incremental cost. As a result, designing consensus parameter α and β can be decoupled from designing regulation service gain ϵ_i . We summarize the design procedure as follow,

Step 1: Design α and β such that the consensus protocol is stable and fast when implemented in discrete time domain.

Step 2: Estimate or obtain the worst case delay τ_{MAX} and a_{MIN} , and design ϵ_{SUM} such that (44) is stable with sufficient stability margin. For example, if a $\pi/4$ phase margin is required, substituting it into the second equation of (45) yields $s = \frac{\pi}{4\tau_{\text{MAX}}}$. Further substituting s into the first equation of (45) yields $\epsilon_{\text{SUM}} = \frac{\pi a_{\text{MIN}}}{2\tau_{\text{MAX}}}$. This controller gain gives a good P_{REG} tracking performance while guaranteeing stability.

Step 3: Depending on the number M of regulation service DGs, set $\epsilon_i = \epsilon_{\text{SUM}}/M$ for regulation service DGs, and $\epsilon_i = 0$ for the rest.

It is worth noting that the information about the worst case delay τ_{MAX} and the DG with smallest cost factor a_i is only required when designing ϵ_i . This information can be estimated or obtained offline and once the control gains are designed, the algorithm is distributed and requires only neighbor's information during operation. It is also worth noting that above design method provides a sufficient but not necessary condition for the system stability.

V. EXPERIMENT RESULTS

In this section we first introduce the MG for testing and a HIL testbed for implementing and testing the proposed algorithm. Then, we present the test results for various cases.

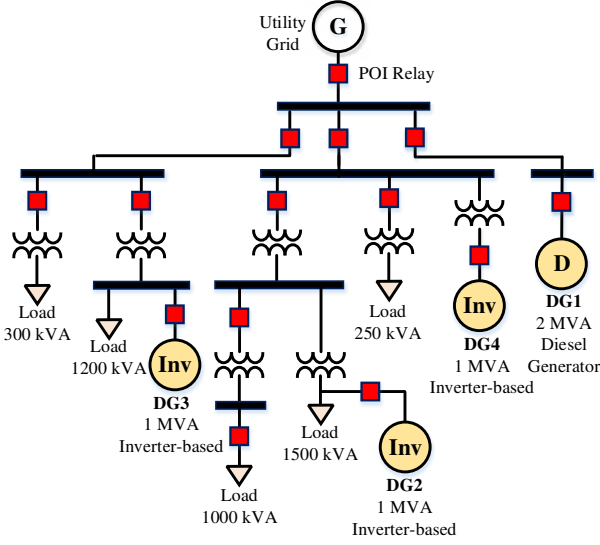


Fig. 7: Microgrid topology for HIL simulation

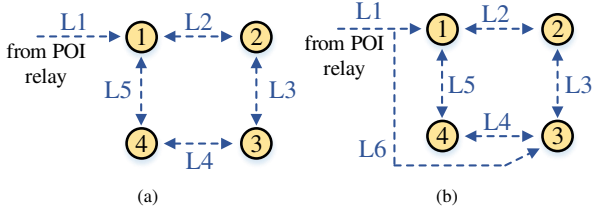


Fig. 8: Communication topology

A. Microgrid for HIL Simulation

We adopt the feeder 1 of Banshee distribution network from [37] as the test MG and add three inverter-based DGs to it, as shown in Fig. 7. Banshee distribution network is a power distribution network that provides a common, general benchmark for testing microgrid control [38]. It includes detailed models and real-world parameters for line impedance, transformers, loads, relays, generators, inverters, etc. Banshee models are open-source and publicly available [39].

The DG parameters are shown in TABLE I. The regulation capacity is 500 kW and the scheduled base load imported from the grid is 1800 kW. Parameters like the line impedance, transformer settings, loads can be found in [37]. The communication network among the DGs and the POI relay is shown in Fig. 8(a). It is worth noting that we use the test MG with four DGs to verify the proposed distributed control algorithm. For such a system, centralized control may be more effective, easier to implement in the field, and have simpler communication network. However, this simple use case serves as a relevant proof-of-concept of the proposed approach.

TABLE I: Microgrid DG Parameters

DG	a	b	c	T_s
DG1 diesel generator	$a = 0.005$	$b = 20$	$c = 0$	$T_s = 167$ ms
DG2 inverter-based	$a = 0.02$	$b = 10$	$c = 0$	$T_s = 167$ ms
DG3 inverter-based	$a = 0.025$	$b = 8$	$c = 0$	$T_s = 167$ ms
DG4 inverter-based	$a = 0.015$	$b = 12$	$c = 0$	$T_s = 167$ ms

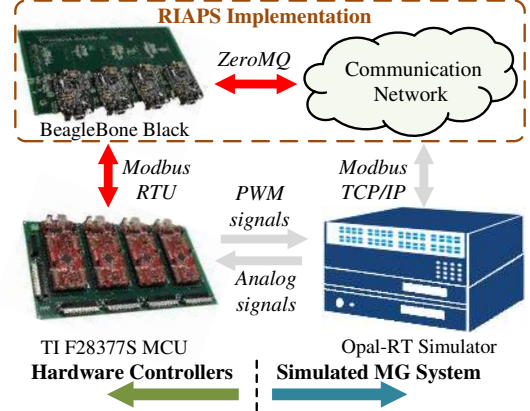


Fig. 9: Real-time HIL Testbed Setup

B. HIL Testbed

The HIL testbed is shown in Fig. 9. OPAL-RT real-time simulator is used to simulate the MG components such as DGs, line impedances, relays, etc. The switching model of the power electronics converters is modeled in the OPAL-RT FPGA-based simulator with a small simulation time step (500 ns), capable of capturing the fast dynamics of the switching components. The non-switching components are modeled in the OPAL-RT CPU-based simulator with a larger simulation time step (65 μ s), allowing for simulating a MG with adequate size in real-time.

The industry-grade micro-controller units (MCUs) TMS320F28377S from Texas Instruments are used to for controlling the inverter-based DGs. The measured DG operation states like voltage and current are sampled by the analog-to-digital converters (ADCs) of the MCUs. Inverter-based DGs' local control, such as current loop, voltage loop, and droop control are implemented in the MCUs. The MCUs send pulse-width modulation (PWM) signals to the OPAL-RT simulator as gate signals for the simulated DGs. In the test MG shown in Fig. 7, DG1 is a diesel generator and its local control is implemented in the OPAL-RT simulator. A detailed description of the generator's local control and parameters can be found in [37]. DG2, DG3, and DG4 are inverter-based and their local control are implemented in the MCUs. The inverter-based DGs operate in voltage control mode whose control includes a current loop, a voltage loop, and droop control. The implemented droop control can be described by

$$f_i^* = f_r - m(P_i - P_i^*) \quad (46)$$

$$V_i^* = V_r - n(Q_i - Q_i^*) - n_s \int (Q_i - Q_i^*) dt \quad (47)$$

where f_r and V_r are the rated frequency and voltage, respectively; P_i^* and Q_i^* are the active power and reactive power commands, respectively. In the tests, P_i^* is the power command received from the EDP algorithm (26) while Q_i^* is set to 0. In (47), one extra integrator term is added to the conventional $Q-V$ droop. This term ensures that the inverter reactive power Q_i can follow its command Q_i^* accurately in grid-connected mode; in islanded mode, this term is removed by setting $n_s = 0$ and (47) is reduced to the conventional droop

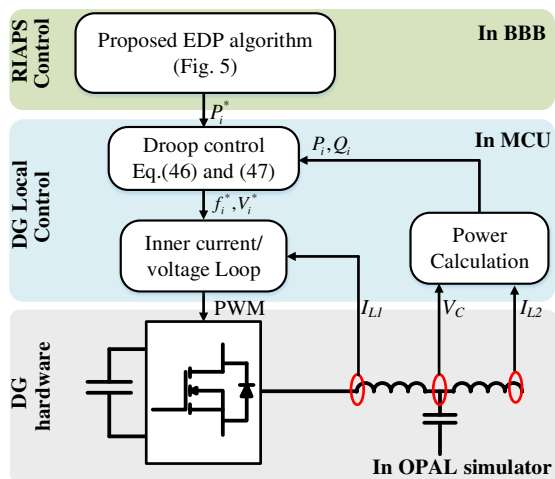


Fig. 10: Overall control diagram for inverter-based DGs

control [40], [41]. The frequency reference f_i^* and voltage reference V_i^* generated by droop control are further used by inner voltage/current loop to control the inverter output voltage. We use PI controller in synchronous dq reference frame for the voltage/current loop. Detailed parameters can be found in Appendix B. With those parameters, the bandwidth for the DG's local active power control is 1.3 Hz.

The proposed distributed EDP algorithm is implemented in the testbed using the Resilient Information Architecture Platform for the Smart Grid (RIAPS). The RIAPS platform is an open-source software platform for distributing computation and communication capability to multiple RIAPS nodes at the edge of the network. Detailed introduction to the RIAPS platform can be found in [42]. The hardware for the RIAPS nodes is beaglebone black board (BBB), featuring a variety of I/Os, adequate processing power, and 100 Mbit/s Ethernet connectivity. Each BBB can communicate with one MCU using Modbus RTU protocol. With this communication link, the power reference is calculated in the BBB and sent to the MCU, which further controls the inverter-based DGs. For DG1 and POI relay, their BBBs use Modbus TCP/IP to communicate with their simulated local controllers in the OPAL-RT simulator, respectively. The communication between different BBBs is realized by the RIAPS platform. The overall control diagram for the inverter-based DG is shown in Fig. 10.

When implementing the proposed control (26)-(29) on the BBBs, it is important to select a time step during which all the computation and communication can be finished. During each time step, the BBB needs to finish three tasks: first, the BBB runs the proposed EDP algorithm; second, the BBB sends a Modbus message to the DGs; third, the BBB shares the consensus variables with its neighbors. We measure the average time required for each task and the results are presented in TABLE II. The average time for all tasks is 36.1817 ms. In practice the actual execution time might be much longer depending on the network delays, other tasks on the node, etc. In the tests, we select 167 ms as time step to guarantee a sufficient margin.

TABLE II: Time for different tasks (averaged over 20000 data points)

Computation	$T_{comp} = 0.2167$ ms
Modbus messaging	$T_{modbus} = 31.6846$ ms
RIAPS messaging	$T_{RIAPS} = 4.2805$ ms

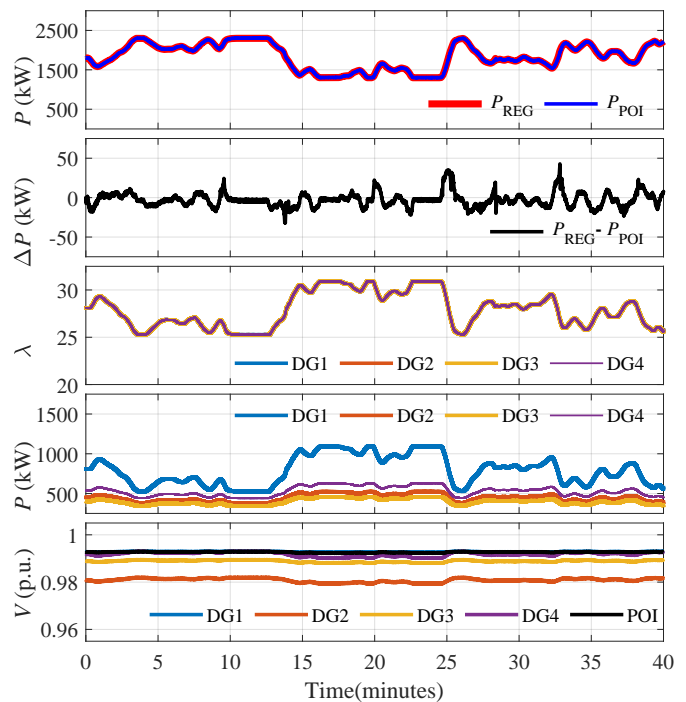


Fig. 11: Case 1 results for the full test RegD signal for 40 minutes.

C. Case Study

In following we show the performance of the proposed algorithm in various scenarios. The performance is evaluated based the two goals: 1) how tightly the POI power follows the RegD power command, i.e., the quality of provided regulation service; 2) how close the incremental costs for DGs are, i.e., the optimality of the EDP solution.

Case 1: Full test for RegD. Fig. 11 shows the results for the 40-minute RegD signal test. The maximum error for POI power tracking $|P_{REG} - P_{POI}|$ is less than 50 kW. The incremental costs λ for all DGs are kept almost the same throughout the test. From the power output plot, it can be observed that DG1 has much higher power output when the combined power demand from the load and regulation service is high. The bottom plot shows the voltage measured at different locations. The voltage at POI is around at 0.99 p.u. throughout the test while the voltages at the DGs have small fluctuations due to the interaction between the line impedance and injected power. The voltage at DG1 is close to the POI voltage because it is connected to the POI bus with a small line impedance, i.e., they have a small electrical distance. The voltage at DG2 is the lowest because the electrical distance between DG2 and POI is the largest among the four DGs. The maximum voltage deviation from the voltage without regulation service is 0.0017 p.u. at DG4. Despite the small fluctuations, all the voltages are within the 5% tolerance. This means providing regulation service does not significantly impact the voltage profile, which validates our first assumption in Subsection IV-B.

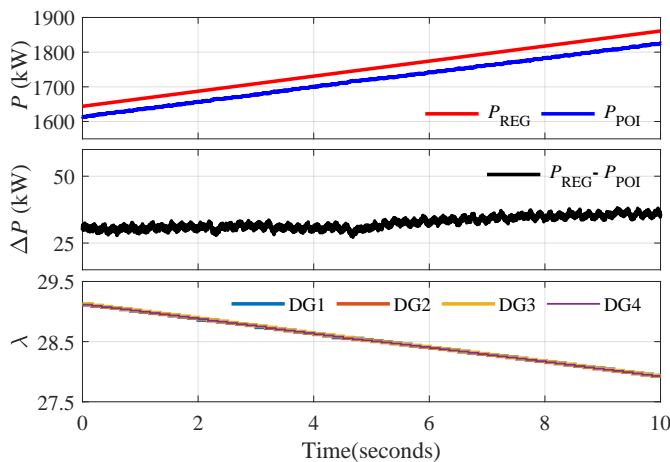


Fig. 12: Case 1 results for the RegD ramp region at point A in Fig. 2.

Based on PJM’s criteria, the overall performance score for the provided regulation service is calculated as the average of following three components,

- Delay score: calculated based on the delay that provides the maximum correlation between the regulation signal and the MG power output change. A delay less than 10 s scores a perfect 1. The test results in Fig. 11 have a delay less than 10 s and the delay score is 1.
- Correlation score: calculated as the correlation between the regulation signal and the MG power output after removing the above delay. The correlation score is 0.9644 for the test results in Fig. 11.
- Precision score: calculated as based on the normalized absolute error between the regulation signal and the MG power output. The precision score is 0.8821 for the test results in Fig. 11.

The overall score for the provided regulation service is 0.9488 which satisfies PJM’s requirement for a score of 0.75 or better. More details about PJM’s performance score and how it is calculated can be found in [43].

Fig. 12 shows the zoomed-in part of the ramp region of RegD, which is at point A in Fig. 2. During this region, the slope of P_{REG} is around 21.75 kW/s. The error $|P_{REG} - P_{POI}|$ is around 31.42 kW. This error can be reduced by selecting large controller gains ϵ_i . However, increasing ϵ_i also reduces the stability margin. In spite of the error in tracking P_{REG} , the provided regulation service satisfies PJM’s requirement and the first goal is achieved.

Fig. 12 also shows the incremental costs for all DGs during the ramp region of RegD. The incremental costs are staircase curves as they are calculated by the RIAPS nodes with a 167 ms time step. The incremental costs keep decreasing following the trend of RegD and all the incremental costs converge to the same value in spite of the fast changing RegD signal. This shows the proposed EDP algorithm can achieve both goals simultaneously.

Case 2: Comparison with dynamic consensus. To demonstrate the improvement of the proposed consensus protocol, we implement the dynamic consensus to solve the EDP, which is widely used in literature (see [10], [15] and [17]). Recall that equation (10) governing the internal variable y_i

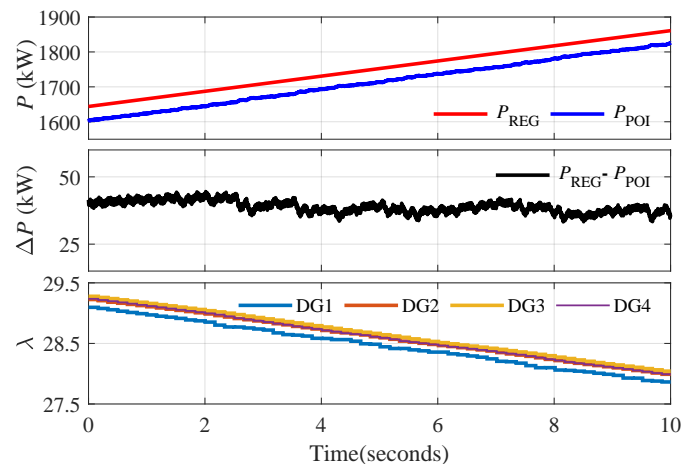


Fig. 13: Case 2 results with dynamic consensus for the RegD ramp region at point A in Fig. 2.

in the proposed protocol is essentially the same equation for dynamic consensus (6). A simple method to implement dynamic consensus in the EDP is to replace (29) with $\lambda_i^* = y_i$. We use the same parameters in TABLE I and communication links in Fig. 8(a) as in Case 1.

Fig. 13 shows test results for the ramp region of RegD with dynamic consensus. Although the regulation power command tracking performance is similar to the proposed method, dynamic consensus fails to converge correctly as the incremental costs are different for different DGs. The system operates at a less economic point. This shows the EDP algorithm based on dynamic consensus cannot achieve the second goal during the ramp region of the regulation signal.

The total operating cost is calculated as,

$$C_{total} = \sum_{t=t_s}^{t_s+T_c} \sum_{i=1}^4 a_i P(t)^2 + b_i P(t) + c_i \quad (48)$$

where T_c is the length of time over which the total operating cost is calculated and t_s determines the starting point for the cost calculation. We define the cost reduction factor of the proposed method comparing to dynamic consensus as,

$$\eta = \frac{C_{total}^{dynamic} - C_{total}^{proposed}}{C_{total}^{dynamic}} \quad (49)$$

We distinguish between two sub-cases. In the first sub-case, the cost reduction factor is calculated for the 40-minute test by setting $T_c = 40$ mins and $t_s = 0$ s in (48). The cost reduction factor is $\eta_1 = 0.15\%$. In the second sub-case, the cost reduction factor is calculated for the 10-second ramp region as shown in Fig. 12 and Fig. 13. The cost reduction factor is $\eta_2 = 0.51\%$. For large systems, this relative cost reduction can lead to significant absolute cost savings. Besides MGs providing regulation service, the proposed method applies to MGs with dynamic internal load profiles, which can also have many ramp regions due to PV generation or dynamic load behavior. Therefore, it is widely applicable to many MG use cases. The cost reduction is obtained by changing the consensus protocol without any extra hardware. This highlights the major advantage of the proposed method, i.e., it can achieve a cost reduction at no additional expense (except a negligible

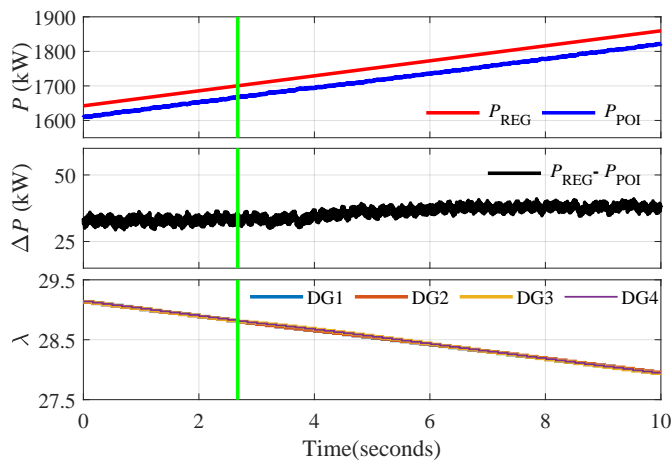


Fig. 14: Case 3 results for loss of communication link L3 at $t = 2.6$ s marked by the green bar.

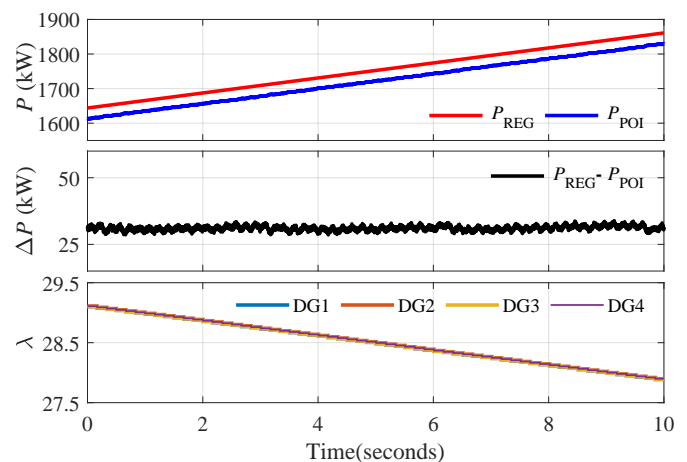


Fig. 16: Case 4 results with gains $\epsilon_1 = \epsilon_3 = 0.01/2$ and $\epsilon_2 = \epsilon_4 = 0$ for the RegD ramp region at point A in Fig. 2.

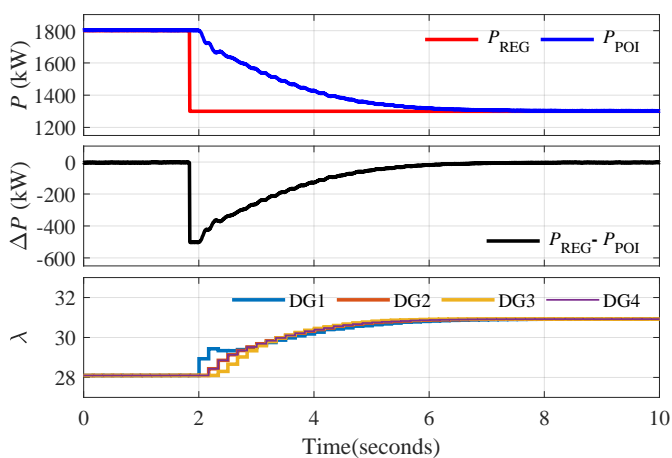


Fig. 15: Case 4 results for enabling the RegD signal at point B in Fig. 2

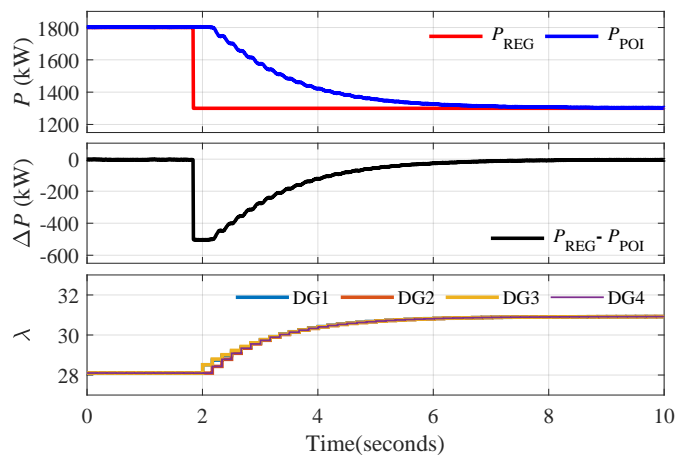


Fig. 17: Case 4 results with gains $\epsilon_1 = \epsilon_3 = 0.01/2$ and $\epsilon_2 = \epsilon_4 = 0$ for enabling the RegD signal at point B in Fig. 2

increase in the computation and communication burden).

Case 3: Communication link failure. In this case we verify the performance of the proposed algorithm under communication link failure. We assume that the communication link L3 fails at $t = 2.6$ s. The results are shown in Fig. 14. Because the proposed consensus protocol (thus the proposed EDP algorithm) only requires a connected communication graph, its performance is not affected by the failure of communication link L3. This is also true if the communication link L2, L4, or L5 fails.

If the communication link L1 fails, the RegD signal cannot be sent to the DGs thus the regulation service cannot be provided correctly. This can be avoided if an extra communication link from the POI relay and DGs is available. An example is shown Fig. 8 (b). More discussion about Fig. 8 (b) can be found in Case 5.

If two communications links out of L2, L3, L4, and L5 fail, the communication graph is disconnected. Similar to any consensus-based distributed algorithms, the proposed control algorithm cannot work properly under this condition; additional communication links among DGs are necessary to achieve higher levels of redundancy.

Case 4: Transient performance. In this case we verify the transient performance of the proposed control by enabling

the regulation service at point B in Fig. 2. Before enabling the service, the POI power is regulated at 1800 kW with $RegD = 0$ and after enabling it, $RegD = -1$ at point B, which corresponds to a -500 kW step change in P_{REG} .

The test results are shown in Fig. 15. The power mismatch is eliminated in less than 5 seconds. The rise time (from 10% to 90% of the 500 kW step response) is 2.9 seconds, which corresponds to a 0.12 Hz bandwidth for the first-order-like step response shown in Fig. 15. Considering the bandwidth of the DG's local active power control (1.3 Hz) is more than 10 times the bandwidth of the proposed algorithm, our assumption 2) in Subsection IV-B is verified: the dynamics of the proposed algorithm are effectively decoupled from the faster dynamics of DGs's local control. The incremental cost of DG1 increases first after enabling the regulation service and the consensus algorithm soon regulates them to the same value.

Case 5: Controller gain design. In this case we verify the gain design method proposed in section IV-C. We set the control gains to $\epsilon_1 = \epsilon_3 = 0.01/2$ and $\epsilon_2 = \epsilon_4 = 0$ such that the sum of control gains ϵ_{SUM} remains the same. This selection of gains means an extra communication link L6 between DG3 and the relay is necessary, as shown in Fig. 8 (b).

After re-running the test for Case 1 and Case 4 with the new gains, the results are shown in Fig. 16 and Fig. 17, respectively.

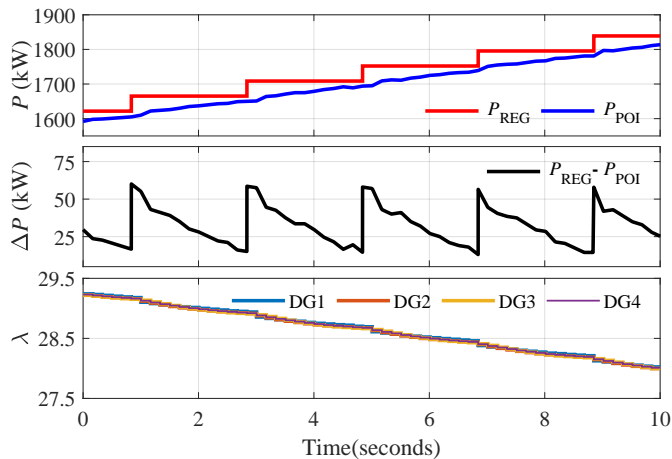


Fig. 18: Case 6 results with discrete regulation signal.

Fig. 16 shows that the error $|P_{REG} - P_{POI}|$ is around 32 kW during the ramp region of the RegD signal. Fig. 17 shows that the error $|P_{REG} - P_{POI}|$ is also similar to that of Case 4 during the transient. This means the new gains' performance of tracking the regulation power command is the same as that of the control gains in TABLE I. This verifies our equivalent model for gain design shown in Fig. 6 as the sum of control gains determines the tracking performance.

Comparing Fig. 17 with Fig. 15, the incremental cost consensus performance during transient is improved as now the inputs $\epsilon_{SUM}(P_{REG} - P_{POI})$ are split between DG1 and DG3. Another advantage of having more non-zero ϵ_i is redundancy. In case the communication link between POI relay and DG1 failed, the POI power can still be regulated. If the link failure can be detected, DG3 can set its new control gain after the failure to $\epsilon_1 + \epsilon_3$ to guarantee the same power tracking performance as before the failure. However, all above advantages comes with the cost of having an extra communication link.

Case 6: Discrete regulation signal. In practice, the RegD signal is received from PJM every 2 seconds. As a result, RegD is a discrete signal with a 2-second time step. In this case, we run the 40-minute full test using a discrete RegD signal while all the other parameters remain the same as in TABLE I. With the discrete RegD signal, the achieved overall score is 0.9534, which is comparable to the score obtained in Case 1. Fig. 18 shows the test results for the ramp region of the discrete RegD signal. Due to the discrete nature, the regulation error $|P_{REG} - P_{POI}|$ reaches about 60 kW at the beginning of each RegD step and decreases to about 15 kW at the end. The incremental costs for all DGs are kept almost the same with some minor transient due to the RegD step. This shows that the proposed algorithm can achieve good regulation service quality and optimal economic dispatch simultaneously for the discrete RegD signal.

Case 7: BESS with constant cost function coefficients. In this case, we verify the performance of the proposed algorithm with the BESS. We simulate a battery at the DC side of the inverter-based DG4. The simulated battery capacity is selected to be 250 kWh to make the SoC fluctuation more significant. The initial SoC is set to 50%. The cost function coefficients

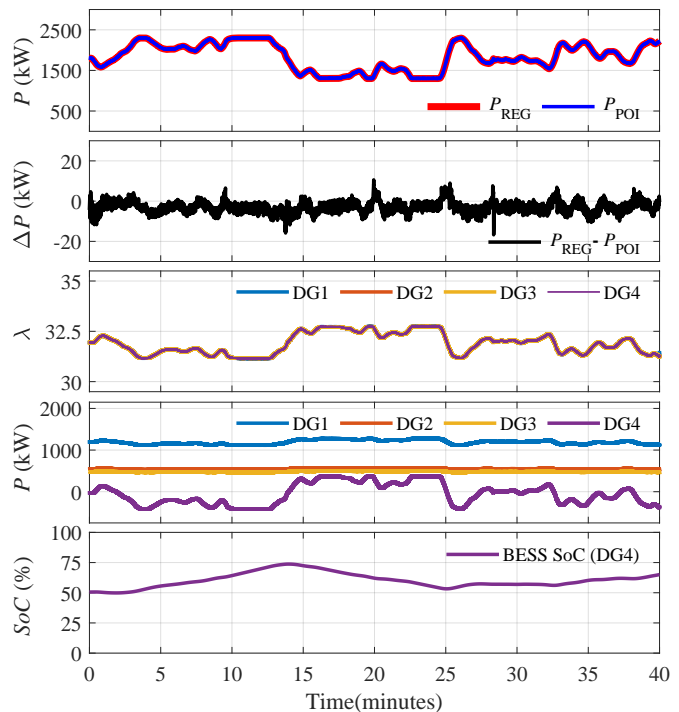


Fig. 19: Case 7 (DG4 is a BESS with constant cost function coefficients) results for the 40-minute RegD test.

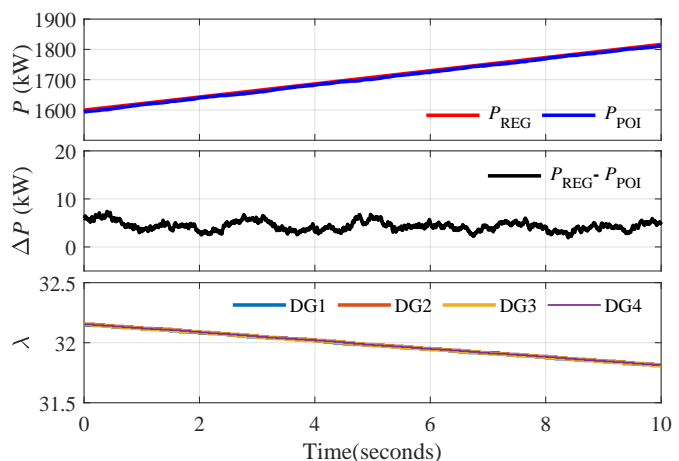


Fig. 20: Case 7 (DG4 is a BESS with constant cost function coefficients) results for the RegD ramp region.

for DG4 are changed to $a = 0.001$, $b = 32$, and $c = 0$ to account for the BESS characteristics while the coefficients for DG1, DG2, and DG3 remain the same as in TABLE I. Throughout the test, the coefficients are constant.

Fig. 19 shows the results for the 40-minute RegD test. It is observed that the POI power follows the regulation power tightly. The maximum error $|P_{REG} - P_{POI}|$ is less than 10 kW, demonstrating better performance than the results without the BESS in Fig. 11. This is because coefficient a for DG4 is smaller than that used in Case 1, which reduces a_{AVE} and results in a better regulation performance as predicted by the equivalent model in Fig. 6. Fig. 20 shows the zoomed-in part of the ramp region of RegD. It further verifies the better performance in tracking regulation power command while achieving the same incremental cost for all DGs. During the

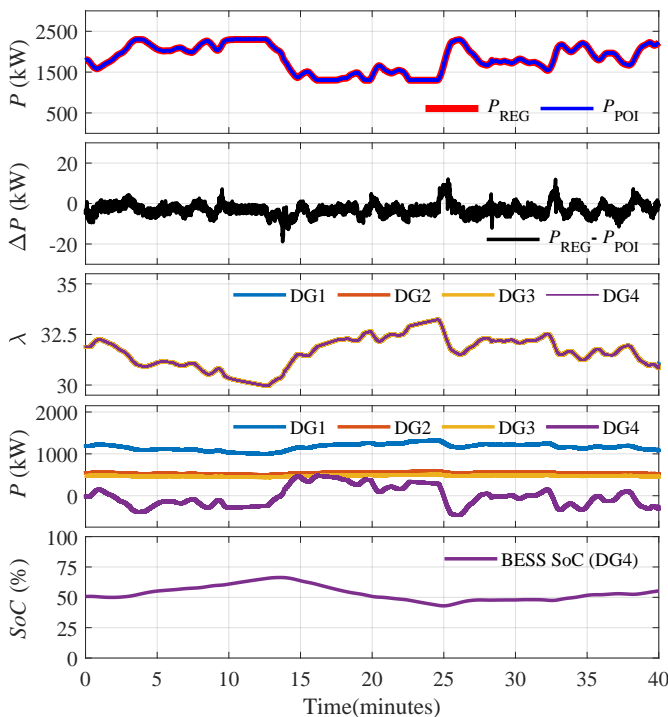


Fig. 21: Case 8 (DG4 is a BESS with SoC-dependent cost function coefficients) results for the 40-minute RegD test.

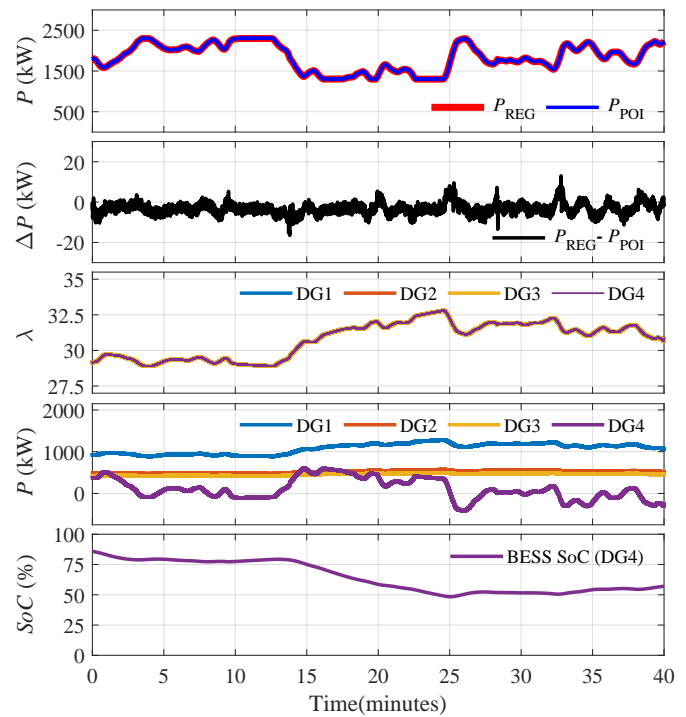


Fig. 23: Case 9 (DG4 is a BESS with SoC-dependent cost function coefficients and 85% initial SoC) results for the 40-minute RegD test.

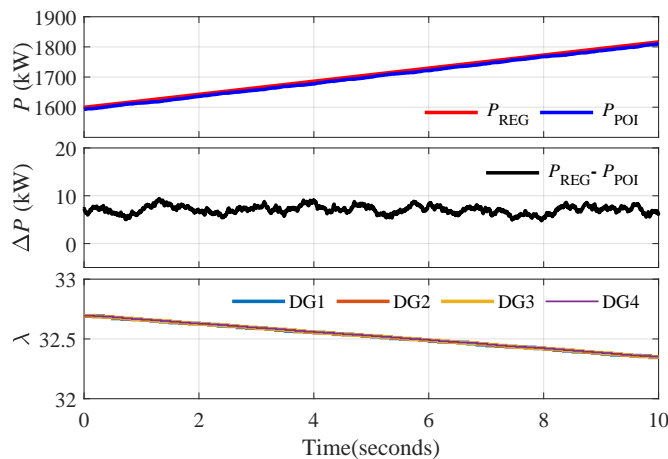


Fig. 22: Case 8 (DG4 is a BESS with SoC-dependent cost function coefficients) results for the RegD ramp region.

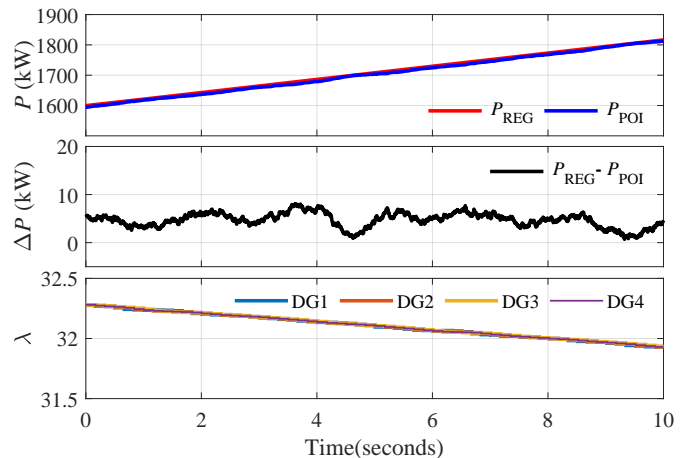


Fig. 24: Case 9 (DG4 is a BESS with SoC-dependent cost function coefficients and 85% initial SoC) results for the RegD ramp region.

test, the highest SoC is 74% at $t = 14$ min while the lowest SoC is the initial SoC (50%). The BESS SoC increases to 65% at the end of the 40-minute test. Without any constraints for the SoC, it cannot be guaranteed that the SoC will stay in a target/safe zone.

Case 8: BESS with SoC-dependent cost function coefficients and 50% initial SoC. In this case, we verify the performance of the proposed algorithm with the BESS which has SoC-dependent cost function coefficients to maintain the SoC at an arbitrarily selected target of 50%. The DGs' configuration and parameters are the same as that in Case 7. The cost coefficients for the BESS are selected as $a = 0.001$, $b = 37 - 10 \times SoC$, $c = 0$ as an example. They can be determined by a higher-level optimization algorithm such as [33]. The initial SoC is 50%.

Fig. 21 shows the results for the 40-minute RegD test. While providing comparable performance in tracking regulation power command as Case 7, the BESS SoC fluctuates around 50% throughout the test. The highest SoC is 66% at $t=14$ min while the lowest SoC is 43% at $t=25$ min. At the end of the test, the SoC is 55%, demonstrating its capability of maintaining the SoC around the 50% target. Fig. 22 shows the zoomed-in part of the ramp region of RegD. The proposed algorithm can achieve the same incremental cost for all DGs with slowly varying cost function coefficients to maintain the BESS SoC.

Case 9: BESS with SoC-dependent cost function coefficients and 85% initial SoC. To further show that the proposed method's capability of maintaining the BESS SoC, the initial SoC is set to 85% while all the other parameters are the same as that in Case 8. The test results are shown in Fig. 23. With a

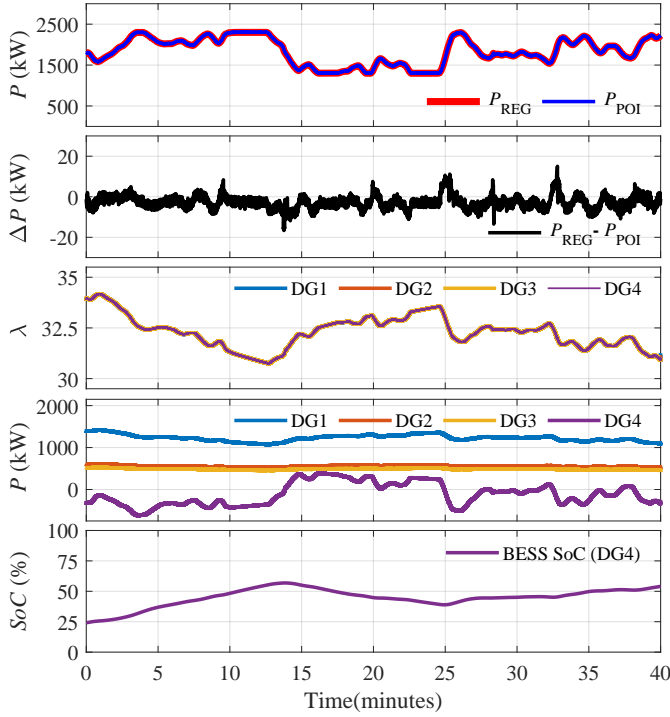


Fig. 25: Case 10 (DG4 is a BESS with SoC-dependent cost function coefficients and 25% initial SoC) results for the 40-minute RegD test.

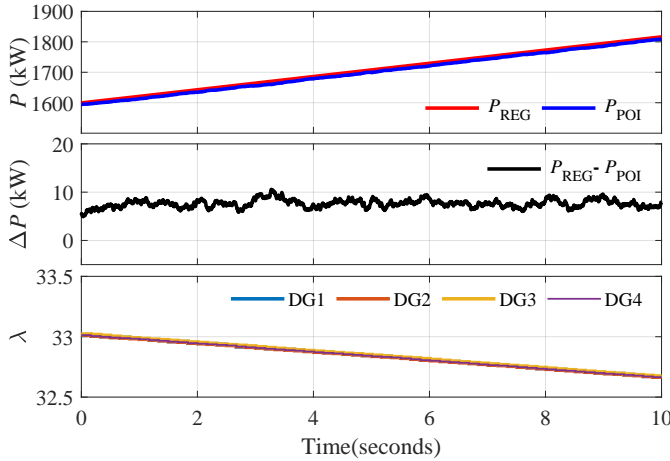


Fig. 26: Case 10 (DG4 is a BESS with SoC-dependent cost function coefficients and 25% initial SoC) results for the RegD ramp region.

high initial SoC, the DG4 power output is reduced during the first 20 minutes of the test to decrease the SoC to around 50%. While maintaining the SoC, DG4's power output follows the trend of the RegD signal to participate in providing regulation service. Throughout the test, the SoC is within 20% - 90% with the highest SoC being the initial SoC. At the end of the test, the SoC is 57%. Fig. 24 shows the zoomed-in part of the ramp region of RegD. The proposed algorithm can achieve the same incremental cost for all DGs with slowly varying cost function coefficients to maintain the BESS SoC.

Case 10: BESS with SoC-dependent cost function coefficients and 25% initial SoC. In this case, the initial SoC is set to 25% while all the other parameters are the same as that in Case 8. The test results are shown in Fig. 25. Due to the low initial SoC, DG4 absorbs power from the MG to increase its SoC to around 50% in the first 10 minutes of the

test. The absorbed power follows the trend of the RegD signal to participate in providing regulation service. Throughout the test, the SoC is within 20% - 90% with the lowest SoC being the initial SoC. At the end of the test, the SoC is 54%. Fig. 26 shows the zoomed-in part of the ramp region of RegD. The proposed algorithm can achieve the same incremental cost for all DGs with slowly varying cost function coefficients to maintain the BESS SoC.

VI. DISCUSSION AND CONCLUSION

When a MG is providing regulation service, the optimal EDP solution changes with the regulation signal. By observing that the regulation signal has ramp regions, we propose a consensus protocol that achieves zero steady-state error for ramp inputs. The proposed protocol is applied to solve EDP for MGs providing regulation service, achieving good regulation service quality and optimal economic dispatch simultaneously. The proposed method can also be used for MGs with dynamic internal load profiles that have many ramp regions.

To consider the BESS in the MGs, we embed the SoC constraints implicitly in the BESS cost function. Case studies presented show that it is possible to control the BESS operation and maintain its SoC using correctly selected cost function coefficients. However, this approach has two potential drawbacks. First, as an implicit constraint, it does not provide an explicit bound for the deviation from the target SoC. Second, the optimal solution to the EDP changes with the coefficients. Therefore, a higher-level optimization algorithm or well-designed rules should be used to determine the coefficients to guarantee that the optimal solution has satisfactory performance. The proposed EDP algorithm (26)-(29) guarantees accurate convergence to the optimal solution. Despite the drawbacks, this approach functions sufficiently well when the BESS coefficients are properly parameterized, as shown by the test results.

APPENDIX A

DERIVATION OF TRANSFER FUNCTION $\mathbf{T}(s)$

$$\begin{aligned} \mathbf{T}(s) &= s \begin{bmatrix} \mathbf{I}_N & \mathbf{0}_{N \times N} \\ \mathbf{0}_{N \times N} & s\mathbf{I}_N + \beta\mathbf{L} \end{bmatrix}^{-1} \begin{bmatrix} s\mathbf{I}_N + \alpha\mathbf{L} & \beta\mathbf{L} \\ \mathbf{0}_{N \times N} & s\mathbf{I}_N + \beta\mathbf{L} \end{bmatrix} \begin{bmatrix} \mathbf{I}_N \\ \mathbf{I}_N \end{bmatrix} \\ &= s \begin{bmatrix} \mathbf{I}_N & \mathbf{0}_{N \times N} \\ \mathbf{0}_{N \times N} & s\mathbf{I}_N + \beta\mathbf{L} \end{bmatrix}^{-1} \begin{bmatrix} (s\mathbf{I}_N + \alpha\mathbf{L})^{-1} & -(s\mathbf{I}_N + \alpha\mathbf{L})^{-1}\beta\mathbf{L}(s\mathbf{I}_N + \beta\mathbf{L})^{-1} \\ \mathbf{0}_{N \times N} & (s\mathbf{I}_N + \beta\mathbf{L})^{-1} \end{bmatrix} \begin{bmatrix} \mathbf{I}_N \\ \mathbf{I}_N \end{bmatrix} \\ &= s \left[(s\mathbf{I}_N + \alpha\mathbf{L})^{-1} - (s\mathbf{I}_N + \alpha\mathbf{L})^{-1}\beta\mathbf{L}(s\mathbf{I}_N + \beta\mathbf{L})^{-1} \right] \\ &= s (s\mathbf{I}_N + \alpha\mathbf{L})^{-1} [\mathbf{I}_N - \beta\mathbf{L}(s\mathbf{I}_N + \beta\mathbf{L})^{-1}] \end{aligned}$$

Substituting $\mathbf{L} = \mathbf{Q}\Psi\mathbf{Q}^T$ and $\mathbf{I}_N = \mathbf{Q}\mathbf{I}_N\mathbf{Q}^{-1}$, and recall $\mathbf{Q}^{-1} = \mathbf{Q}^T$,

$$\begin{aligned} \mathbf{T}(s) &= s\mathbf{Q}(s\mathbf{I}_N + \alpha\Psi)^{-1} [\mathbf{I}_N - \beta\Psi(s\mathbf{I}_N + \beta\Psi)^{-1}] \mathbf{Q}^T \\ &= \sum_{i=1}^N \frac{s}{s + \alpha\psi_i} \left(1 - \frac{\beta\psi_i}{s + \beta\psi_i} \right) \mathbf{q}_i \mathbf{q}_i^T \\ &= \sum_{i=1}^N \frac{s^2}{(s + \alpha\psi_i)(s + \beta\psi_i)} \mathbf{q}_i \mathbf{q}_i^T \end{aligned}$$

APPENDIX B
PARAMETERS FOR INVERTER-BASED DGs

TABLE III: Parameters for Inverter-based DGs

Parameters		Values
General	Rated power output (S^*)	1 MW
	DC link voltage (V_{DC})	1200 V
	Switching frequency (f_{SW})	5 kHz
LCL filter	Inverter side inductor (L_1)	150 μ H
	Capacitor (C)	800 μ F
	Grid side inductor (L_2)	300 μ H
Droop control	Low pass filter cut-off frequency (f_{lfp})	8 Hz
	P-f droop gain (m)	1 Hz/MW
	Q-V droop gain (n)	25 V/MVar
	Q-V integrator gain (n_s)	1×10^{-3}
	Rated peak voltage (V_r)	392 V
	Rated frequency (f_r)	60 Hz
Inner loop	Voltage loop PI gains ($k_{P,V}, k_{I,V}$)	4.86, 1260
	Current loop PI gains ($k_{P,I}, k_{I,I}$)	0.31, 50

REFERENCES

[1] D. T. Ton and M. A. Smith, "The us department of energy's microgrid initiative," *The Electricity Journal*, vol. 25, no. 8, pp. 84–94, 2012.

[2] A. Majzoobi and A. Khodaei, "Application of microgrids in providing ancillary services to the utility grid," *Energy*, vol. 123, pp. 555–563, 2017.

[3] L. Yavuz, A. Önen, S. Muyeen, and I. Kamwa, "Transformation of microgrid to virtual power plant—a comprehensive review," *IET Generation, Transmission & Distribution*, vol. 13, no. 11, pp. 1994–2005, 2019.

[4] M. L. Di Silvestre, P. Gallo, M. G. Ippolito, R. Musca, E. Riva Sanseverino, Q. T. T. Tran, and G. Zizzo, "Ancillary services in the energy blockchain for microgrids," *IEEE Transactions on Industry Applications*, vol. 55, no. 6, pp. 7310–7319, 2019.

[5] A. J. Wood, B. F. Wollenberg, and G. B. Sheblé, *Power generation, operation, and control*. John Wiley & Sons, 2013.

[6] J. W. Simpson-Porco, Q. Shafiee, F. Dörfler, J. C. Vasquez, J. M. Guerrero, and F. Bullo, "Secondary frequency and voltage control of islanded microgrids via distributed averaging," *IEEE Transactions on Industrial Electronics*, vol. 62, no. 11, pp. 7025–7038, 2015.

[7] F. Dörfler, J. W. Simpson-Porco, and F. Bullo, "Breaking the hierarchy: Distributed control and economic optimality in microgrids," *IEEE Transactions on Control of Network Systems*, vol. 3, no. 3, pp. 241–253, 2016.

[8] Z. Cheng, J. Duan, and M.-Y. Chow, "To centralize or to distribute: That is the question: A comparison of advanced microgrid management systems," *IEEE Industrial Electronics Magazine*, vol. 12, no. 1, pp. 6–24, 2018.

[9] M. Hosseinzadeh, L. Schenato, and E. Garone, "A distributed optimal power management system for microgrids with plug&play capabilities," *Advanced Control for Applications*, vol. 3, no. 1, p. e65, 2021.

[10] Z. Zhang and M. Chow, "Convergence analysis of the incremental cost consensus algorithm under different communication network topologies in a smart grid," *IEEE Transactions on Power Systems*, vol. 27, no. 4, pp. 1761–1768, 2012.

[11] J. Hu, J. Duan, H. Ma, and M.-Y. Chow, "Distributed adaptive droop control for optimal power dispatch in dc microgrid," *IEEE Transactions on Industrial Electronics*, vol. 65, no. 1, pp. 778–789, 2018.

[12] X. Lu, S. Xia, G. Sun, J. Hu, W. Zou, Q. Zhou, M. Shahidehpour, and K. W. Chan, "Hierarchical distributed control approach for multiple on-site ders coordinated operation in microgrid," *International Journal of Electrical Power & Energy Systems*, vol. 129, p. 106864, 2021.

[13] Q. Li, D. W. Gao, H. Zhang, Z. Wu, and F.-y. Wang, "Consensus-based distributed economic dispatch control method in power systems," *IEEE Transactions on Smart Grid*, vol. 10, no. 1, pp. 941–954, 2019.

[14] Z. Wang, W. Wu, and B. Zhang, "A fully distributed power dispatch method for fast frequency recovery and minimal generation cost in autonomous microgrids," *IEEE Transactions on Smart Grid*, vol. 7, no. 1, pp. 19–31, 2016.

[15] S. Yang, S. Tan, and J.-X. Xu, "Consensus based approach for economic dispatch problem in a smart grid," *IEEE Transactions on Power Systems*, vol. 28, no. 4, pp. 4416–4426, 2013.

[16] S. Kawamura, K. Cai, M. Ye, and Z. Lin, "Tight bound on parameter of surplus-based averaging algorithm over balanced digraphs," *International Journal of Control*, vol. 93, no. 8, pp. 1859–1866, 2020.

[17] Y. Yan, Z. Chen, V. Varadharajan, M. J. Hossain, and G. E. Town, "Distributed consensus-based economic dispatch in power grids using the paillier cryptosystem," *IEEE Transactions on Smart Grid*, vol. 12, no. 4, pp. 3493–3502, 2021.

[18] Y. Du, H. Tu, X. Lu, and S. Lukic, "Privacy-preserving distributed average observers in distribution systems with grid-forming inverters," *IEEE Transactions on Smart Grid*, pp. 1–1, 2021.

[19] D. P. Spanos, R. Olfati-Saber, and R. M. Murray, "Dynamic consensus on mobile networks," in *IFAC world congress*. Citeseer, 2005, pp. 1–6.

[20] A. Cherukuri and J. Cortés, "Distributed coordination for economic dispatch with varying load and generator commitment," in *2014 52nd Annual Allerton Conference on Communication, Control, and Computing (Allerton)*, 2014, pp. 475–482.

[21] R. A. Freeman, P. Yang, and K. M. Lynch, "Stability and convergence properties of dynamic average consensus estimators," in *Proceedings of the 45th IEEE Conference on Decision and Control*, 2006, pp. 338–343.

[22] C. N. Taylor, R. W. Beard, and J. Humpherys, "Dynamic input consensus using integrators," in *Proceedings of the 2011 American Control Conference*, 2011, pp. 3357–3362.

[23] S. S. Kia, J. Cortés, and S. Martinez, "Dynamic average consensus under limited control authority and privacy requirements," *International Journal of Robust and Nonlinear Control*, vol. 25, no. 13, pp. 1941–1966, 2015.

[24] H. Bai, R. A. Freeman, and K. M. Lynch, "Robust dynamic average consensus of time-varying inputs," in *49th IEEE Conference on Decision and Control (CDC)*, 2010, pp. 3104–3109.

[25] L. Wang and F. Xiao, "Finite-time consensus problems for networks of dynamic agents," *IEEE Transactions on Automatic Control*, vol. 55, no. 4, pp. 950–955, 2010.

[26] F. Chen, Y. Cao, and W. Ren, "Distributed average tracking of multiple time-varying reference signals with bounded derivatives," *IEEE Transactions on Automatic Control*, vol. 57, no. 12, pp. 3169–3174, 2012.

[27] P. Bevilacqua, S. Perrella, R. Bruno, and N. Arcuri, "An accurate thermal model for the pv electric generation prediction: long-term validation in different climatic conditions," *Renewable Energy*, vol. 163, pp. 1092–1112, 2021.

[28] Y. Li, S. Zhang, R. Hu, and N. Lu, "A meta-learning based distribution system load forecasting model selection framework," *Applied Energy*, vol. 294, p. 116991, 2021.

[29] "Regulation market." [Online]. Available: <https://learn.pjm.com/three-priorities/buying-and-selling-energy/ancillary-services-market/regulation-market> [Accessed 12-Feb-2022]

[30] G. Binetti, A. Davoudi, F. L. Lewis, D. Naso, and B. Turchiano, "Distributed consensus-based economic dispatch with transmission losses," *IEEE Transactions on Power Systems*, vol. 29, no. 4, pp. 1711–1720, 2014.

[31] G. Hug, S. Kar, and C. Wu, "Consensus + innovations approach for distributed multiagent coordination in a microgrid," *IEEE Transactions on Smart Grid*, vol. 6, no. 4, pp. 1893–1903, 2015.

[32] D. E. Olivares, A. Mehrizi-Sani, A. H. Etemadi, C. A. Cañizares, R. Iravani, M. Kazerani, A. H. Hajimiragha, O. Gomis-Bellmunt, M. Saeedifard, R. Palma-Behnke, G. A. Jiménez-Estévez, and N. D. Hatziargyriou, "Trends in microgrid control," *IEEE Transactions on Smart Grid*, vol. 5, no. 4, pp. 1905–1919, 2014.

[33] Q. Jiang, M. Xue, and G. Geng, "Energy management of microgrid in grid-connected and stand-alone modes," *IEEE Transactions on Power Systems*, vol. 28, no. 3, pp. 3380–3389, 2013.

[34] R. Olfati-Saber and R. Murray, "Consensus problems in networks of agents with switching topology and time-delays," *IEEE Transactions on Automatic Control*, vol. 49, no. 9, pp. 1520–1533, 2004.

[35] A. P. Seyranian and A. A. Mailybaev, *Multiparameter Stability Theory with Mechanical Applications*. WORLD SCIENTIFIC, 2003.

[36] K. Cai and H. Ishii, "Average consensus on general strongly connected digraphs," *Automatica*, vol. 48, no. 11, pp. 2750–2761, 2012.

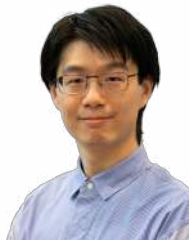
[37] R. Salcedo *et al.*, "Banshee distribution network benchmark and prototyping platform for hardware-in-the-loop integration of microgrid and device controllers," *The Journal of Engineering*, vol. 2019, no. 8, pp. 5365–5373, 2019.

[38] B. Lundstrom. Nrel microgrid challenge. [Online]. Available: <https://erigrid.eu/wp-content/uploads/2017/09/NREL-Microgrid-Challenge-Blake-Lundstrom-NREL.pdf> [Accessed 12-Feb-2022]

[39] M. I. of Technology. Electric power hil controls consortium repository. [Online]. Available: <https://github.com/PowerSystemsHIL/EPHCC> [Accessed 12-Feb-2022]

[40] Y. Li, D. Vilathgamuwa, and P. C. Loh, "Design, analysis, and real-time testing of a controller for multibus microgrid system," *IEEE Transactions on Power Electronics*, vol. 19, no. 5, pp. 1195–1204, 2004.

- [41] H. Tu, Y. Du, H. Yu, S. Lukic, M. Metelko, P. Volgyesi, A. Dubey, and G. Karsai, "A hardware-in-the-loop real-time testbed for microgrid hierarchical control," in *2018 IEEE Energy Conversion Congress and Exposition (ECCE)*, 2018, pp. 2053–2059.
- [42] H. Tu, Y. Du, H. Yu, A. Dubey, S. Lukic, and G. Karsai, "Resilient information architecture platform for the smart grid: A novel open-source platform for microgrid control," *IEEE Transactions on Industrial Electronics*, vol. 67, no. 11, pp. 9393–9404, 2020.
- [43] *PJM Manual 12: Balancing Operations*, Revision 42, PJM, 2021. [Online]. Available: <https://www.pjm.com/-/media/documents/manuals/m12.ashx> [Accessed 12-Feb-2022]



Hao Tu (S'17-M'21) received his bachelor's, master's and Ph.D. degree from Xi'an Jiaotong University, China in 2012, RWTH Aachen University, Germany in 2015, and North Carolina State University, USA in 2020, respectively, all in electrical engineering. He is currently a Research Assistant Professor with the National Science Foundation Future Renewable Electric Energy Delivery and Management (FREEDM) Systems Engineering Research Center, headquartered at North Carolina State University. His research interests include control of

power electronics converters, energy storage systems, microgrids, and machine learning. He is the recipient of the Second Prize Best Paper Award in IEEE Transactions on Transportation Electrification 2021.



Yuhua Du (S'17-M'21) received the B.S. degree in electrical engineering from Xi'an Jiaotong University, China in 2013 and Ph.D. degree in electrical and computer engineering from North Carolina State University, USA in 2019. He was a Research Aide with Argonne National Laboratory in 2018. In February 2022, he joined the College of Automation at Northwestern Polytechnical University as a Professor. His research interests include voltage source converter modeling and control, microgrid distributed secondary control and microgrid

hardware-in-the-loop testbed.

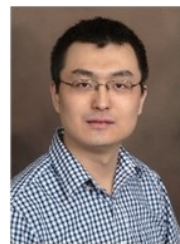


Hui Yu (S'17-M'20) completed the bachelor's and master's degrees from Huazhong University of Science and Technology, Wuhan, China, in 2013 and 2016, respectively, and the Ph.D. degree from North Carolina State University, Raleigh, NC, USA, in 2020, all in electrical engineering. From January 2021 to April 2022, he was a Postdoctoral Research Scholar with the Future Renewable Electric Energy Delivery and Management Systems Center, North Carolina State University. He is currently a Controls Engineer at Medium Voltage R&D, Danfoss Drives,

Research Triangle Park, NC, USA. His research interests include microgrids, renewable energy systems and medium voltage high power converters.



Shweta Meena received her Bachelor's degree from Indian Institute of Technology (IIT) Delhi, India in 2020 in electrical engineering (Power and Automation). She is currently a PhD candidate at the National Science Foundation Future Renewable Electric Energy Delivery and Management (FREEDM) Systems Engineering Research center located in North Carolina State University, Raleigh. Her research interest lies in control and optimization of microgrids.



Xiaonan Lu (S'12-M'13) received his B.E. and Ph.D. degrees in electrical engineering from Tsinghua University, Beijing, China, in 2008 and 2013, respectively. From September 2010 to August 2011, he was a guest Ph.D. student at the Department of Energy Technology, Aalborg University, Denmark. From October 2013 to December 2014, he was a Postdoc Research Associate at the Department of Electrical Engineering and Computer Science, University of Tennessee, Knoxville. From January 2015 to July 2018, he was with Argonne National

Laboratory, first as a Postdoc Appointee and then as an Energy Systems Scientist. In July 2018, he joined the College of Engineering at Temple University as an Assistant Professor. His research interests include modeling and control of power electronic inverters, hybrid AC and DC microgrids, and real-time hardware-in-the-loop simulation. Dr. Lu is the Associate Editor of IEEE Transactions on Industrial Electronics, the Associate Editor of IEEE Transactions on Industry Applications, and the Editor of IEEE Transactions on Smart Grid. He serves as the Chair of the Industrial Power Converters Committee (IPCC) in the IEEE Industry Applications Society (IAS). He is named the Loretta C. Duckworth Faculty Fellow at Temple University, and he is also the recipient of the 2020 Young Engineer of the Year Award in the IEEE Philadelphia Section.



Srdjan Lukic (M'07-SM'19) received the Ph.D. degree in electrical engineering from the Illinois Institute of Technology, Chicago, IL, USA, in 2008, and is currently a Professor and University Faculty Scholar with the Department of Electrical and Computer Engineering, North Carolina State University, Raleigh, NC, USA. He serves as the Deputy Director of the National Science Foundation Future Renewable Electric Energy Delivery and Management (FREEDM) Systems Engineering Research Center, headquartered at North Carolina State University. His current research interests include design, and control of power

electronic converters and electromagnetic energy conversion with application to microgrids, wireless power transfer, energy storage systems, and electric automotive systems. He was a Distinguished Lecturer with the IEEE Vehicular Technology Society from 2011 to 2015.